International Journal of Earth Sciences (2023) 112:1203–1226
https://doi.org/10.1007/s00531-023-02294-6

ORIGINAL PAPER

Thermochronological constraints on the post-Variscan exhumation history of the southeastern Bohemian Massif (Waldviertel and Weinsberg Forest, Austria): palaeogeographic and geomorphologic implications

Ewald Hejl[1] · Bianca Heberer[1] · Bernhard Salcher[1] · Gert Sekyra[1] · Peter Van den haute[2] · Jaromír Leichmann[3]

Received: 28 September 2022 / Accepted: 16 January 2023 / Published online: 15 February 2023

Abstract

Resolving the Mesozoic and Cenozoic palaeogeography and geomorphologic development of outcropping Variscan basement is a pre-condition for the understanding of central European geodynamics. For our study, we have applied apatite fission-track (AFT) and apatite (U–Th)/He (AHe) thermochronology to surface rocks of the southeastern Bohemian Massif. 46 samples were examined by the AFT method. Additional AHe dating was applied to 8 of them. The AFT ages range from 251 ± 46 to 60.2 ± 4.8 Ma. AHe ages range from 25 to 525 Ma with rather high intra-sample scatter. On a regional scale, the AFT ages generally decrease from mainly late Variscan in the NE to Late Cretaceous and Paleocene in the SW. This regional age asymmetry relative to the NW–SE trending watershed of the Weinsberg Forest is neither compatible with regional uplift of a single block nor with large-scale lithospheric updoming. The lack of age breaks along late Variscan faults demonstrates that strong vertical offset cannot have occurred in Cretaceous and Cenozoic times. Inverse modeling of thermochronological data indicates regional Early Cretaceous cooling and subsequent reheating during the Late Cretaceous. Rocks of the present-day surface were heated up to a temperature of ca. 80 °C without full reset of the AFT system. This thermal history is compatible with the existence of a large mainland in Early Cretaceous times and a subsequent sedimentary reburial until the Campanian on the order of up to 1 km overburden. Parts of the exhumed weathering basal relief to the N and NE of the Weinsberg Forest are inherited as 'sealed relief' from Middle Cretaceous time. The observed regional asymmetry of AFT data is best explained by the development of a continental escarpment adjacent to the North Penninic Ocean in latest Cretaceous to Paleogene times. A final episode of accelerated cooling after ca. 20 Ma, as indicated by thermochronological modeling, is tentatively ascribed to either collisional coupling of the Alpine-Carpathian nappe pile with its northern foreland or to East-Alpine slab detachment.

Keywords Apatite fission-track dating · Apatite (U–Th)/He dating · Bohemian Massif · Geomorphology · Passive margin · Escarpment

Introduction

Post-Variscan thermal evolution and exhumation history of the Bohemian Massif has already been investigated in several areas. Vercoutere (1994), Wagner et al. (1994) and Hejl et al. (1997) have applied apatite fission-track (AFT) dating to the Naab mountains and to the basement adjacent to the Franconian Fault in Bavaria. Glasmacher et al. (2002) investigated the thermal history of Upper Proterozoic to Upper Carboniferous formations of the Teplá-Barrandium in the Czech Republic based on modeling of AFT data. Such data and corresponding modeling results are also available for

✉ Ewald Hejl
ewald.hejl@plus.ac.at

[1] Fachbereich für Umwelt und Biodiversität, Paris Lodron Universität Salzburg, Hellbrunnerstraße 34, 5020 Salzburg, Austria

[2] Department of Geology, Ghent University, Krijgslaan 281, 9000 Ghent, Belgium

[3] Department of Geological Sciences, Faculty of Science, Masaryk University, Kotlářská 267/2, 611 37 Brno, Czech Republic

the Ruhla crystalline complex in Thuringia (Thomson and Zeh 2000), for the Erzgebirge (Ventura and Lisker 2003) and the Lusatian Block in Saxony (Ventura et al. 2009), for the Sudetes (Aramowicz et al. 2006; Danišik et al. 2012; Sobczyk et al. 2020), for the south-eastern Bohemian Massif in Austria (Hejl et al. 2003) and for the Bavarian Forest (Siebel et al. 2009; Vamvaka et al. 2014). Both zircon (U–Th)/He thermochronology and AFT analysis were applied to Lower Carboniferous greywackes of the Moravo-Silesian Culm Basin (Botor 2014; Botor et al. 2017). In a recently published, comprehensive study, von Eynatten et al. (2021) have presented new apatite fission-track and (U–Th)/He data for more than 100 samples from central Germany (eastern Rhenish Massif, Harz Mountains, Thuringian Forest, western Bohemian Massif, Franconian Platform, Buntsandstein uplands in northern Hesse and southern Lower Saxony). They interpreted these data together with several hundred, formerly published AFT data from the Rhenish Massif, the Vosges, the Black Forest, the entire Bohemian Massif and the Holy Cross Mountains in Poland. Von Eynatten et al. (2021) concluded that Late Cretaceous to Paleocene exhumation and cooling predominates in many areas and that the spatial exhumation pattern is governed by thrust-bordered basement uplift and superimposed regional domal uplift. In addition to crustal thickening by intraplate compressional stresses, also upwelling asthenosphere is supposed to have contributed to the total amount of uplift and exhumation.

The present investigation aims at a better understanding of the post-Variscan history of the Waldviertel and the Weinsberg Forest (Austria), including its regional exhumation and its tectonic and geomorphologic development. The pilot study of Hejl et al. (2003) has already detected some regional variations in the area's cooling history, but sampling was restricted to an E–W profile along the Kamp valley and a small region further south, in the vicinity of the towns of Krems and Spitz. Triassic AFT ages were found for the Moravian Thaya window, and mainly Cretaceous ages further to the W and S. No discernible age breaks were observed at the Diendorf and Vitis Faults. Thus, significant vertical offset due to these faults is precluded for Cretaceous and Cenozoic times. Furthermore, an integrated study of Eberts et al. (2021) based on Bouguer gravity anomaly, topographic data, low-temperature thermochronology and metamorphic grades in the SW Bohemian Massif has revealed a mainly late- to early post-Variscan age of basement segmentation and differential uplift along the NW–SE striking Pfahl and Danube shear zones in Bavaria. Evidence for Cretaceous and/or Cenozoic vertical offset was found for the NNW–SSE striking Cham Fault.

Thermochronological modeling based on AFT ages and track length data has shown that a regional sedimentary reburial of the Waldviertel basement during the Late Cretaceous is consistent with the data set (Hejl et al. 2003). However, this area was not well covered by thermochronological data—especially samples from the eastern Weinsberg Forest and the Danube tributaries to its S and SW were missing. With 46 instead of 19 samples, the data set of the present investigation covers a larger area and yields a better spatial resolution of the regional cooling trends.

Besides a better resolution of post-Variscan exhumation trends, our study intends to set up well-defined boundary conditions for the thermal evolution, vertical movements, long-term denudation and burial of the Bohemian Massif in a wider, central European context. The post-Variscan cooling history of crustal segments depends on heat flow and geothermal gradients, as well as on exhumation produced by either large-scale domal uplift or by more localized processes like thrusting or fault-scarp tectonics (or a combination of both). Nielsen et al. (2005) have suggested that plate-wide stress relaxation could explain Paleocene basin inversions in Europe. Regional updoming may be due to tectonic thickening by compression, to lithospheric folding (Cloetingh and Burov 2011; Cloetingh et al. 1999), to underplating by basaltic melts (Brodie and White 1994), to thinning of the lithospheric mantle (Meier et al. 2016) or to dynamic topography caused by mantle upwelling (Braun et al. 2013). Von Eynatten et al. (2021) have argued that crustal shortening by compression would have been insufficient to explain the full amplitude of the Late Cretaceous and Paleogene exhumation (often in excess of 4 km) in central Europe, because crustal thickening associated with inversion tectonics can only contribute to half of the doming signal. Therefore, they suggested additional uplift caused by upwelling asthenosphere. We suppose that a denser net of thermochronological data will provide a better resolution and understanding of such processes.

Our new thermochronological age constraints are combined with compiled data from regional stratigraphy, structural geology and geomorphology to deduce the cooling and exhumation history of this former passive margin and its hinterland. Regarding the area under discussion (Waldviertel and the area to the east of Linz), the reader is referred to paleogeographic syntheses of Ziegler (1990), Faupl (1997) and Park (2014). The state of geomorphologic research in the granite domains of the Waldviertel has been reviewed in detail by Huber (1996) who specially emphasized features of the exhumed weathering basal relief. Regional age distributions and the modeled cooling histories that were found by the present investigation, partly confirm former concepts but also depict some trends of the macro-relief development, which were unknown so far. The most important finding is the discovery of an ancient escarpment at the southwestern edge of the Weinsberg Forest. This escarpment has developed adjacent to the passive continental margin of the North Penninic Ocean in Paleogene times. It formed the transition zone between the shelf area (underneath the present-day

North Alpine Molasse) and the exhumed weathering basal relief of a Mesozoic peneplain on top of the Weinsberg Forest and further north, in the Kamp and Thaya catchment area.

Basement geology and geomorphological features

The Variscan basement is mainly composed of Moldanubian nappes, Moravian units of the Thaya Window (adjacent to the Diendorf Fault), and plutonic rocks of the South Bohemian batholith (Fig. 1; cf. also Schnabel et al. 2002). A Grenvillian cratonic provenance of the original Moravo-Silesian crust was suggested by SHRIMP dating of inherited zircons in metagranitoid rocks which has revealed Mesoproterozoic and late Paleoproterozoic tectono-magmatic events (Friedl et al. 2000). On the other hand, the Moldanubian units are characterized by Neoproterozoic and Eburnian (middle Paleoproterozoic) ages of inherited zircon populations (Friedl et al. 2000, 2004; Finger et al. 2007).

The Upper Moravian nappe comprises the Bittesch orthogneiss with U/Pb age 580 ± 7 Ma (Friedl 1997). Eastward thrusting of Moldanubian units onto Moravo-Silesian crust occurred in the Early Carboniferous and produced a distinct metamorphic zonation in the lower plate (Höck 1975, 1994).

The Moldanubian zone of the Waldviertel consists of a Variscan nappe pile. Remarkable formations of this nappe pile are the Dobra gneiss (Drosendorf nappe) with a protolith age of 1.38 ± 0.01 Ga (Gebauer and Friedl 1993; Lindner et al. 2020), and the granulites on top of the Gföhl nappe, which were produced by a high-pressure, high temperature (HPHT) metamorphism at ~ 340 Ma (Kröner et al. 1988; Friedl et al. 1994). Intra-Moldanubian nappe stacking slightly postdates this metamorphic event but was finished before 335 Ma (Friedl et al. 2011; Finger et al. 2007).

Several generations of granitoid intrusions build up the South Bohemian Batholith (Frasl and Finger 1991). The volumetrically dominant, coarse-grained Weinsberg granite intruded between ca. 331 and 322 Ma (± ca. 3 Ma each; Finger et al. 2022). The Eisgarn granite with S-type composition and some fine-grained granites with I-type composition postdate the emplacement of the Weinsberg granite and occupy smaller areas of the batholith (Frasl and Finger 1991; Finger et al. 2022).

Prominent late Variscan faults dissect the Bohemian Massif (Fig. 1a). The area of investigation (Fig. 1b) is affected by the SW-NE trending Diendorf, Vitis, and Rodl Faults. Their shear zones that are exposed at the present-day surface, were formed at different synkinematic paleotemperatures. Mylonites of the Rodl Fault were formed under ductile greenschist facies conditions, but rather cool brittle deformation features are observed along the Diendorf Fault (Brandmayr et al. 1995; Tollmann 1985). The latter has a length of more than 80 km extending from the Alpine foreland in the SW to the southern end of the Boskovice furrow in Moravia. It produced a sinistral strike-slip displacement of almost 60 km (Schermann 1966; Finger and Riegler 1999). Field evidence for Quaternary faulting ca. 25 km to the SW of Brno (Moravia, Czech Republic) was reported by Leichmann and Hejl (1996).

The post-Variscan sediments covering the margins of the Bohemian Massif will be considered in a following section (Mesozoic and Cenozoic paleogeography) with regard to potential reburial and regional erosion. Intensive tropical weathering, strong erosion and peneplanation affected the Bohemian Massif in Meozoic and Cenozoic times. Several stages of peneplanation interacted with shallow-marine ingressions during the Late Jurassic, the Middle to Late Cretaceous and the Miocene (cf. Hejl et al. 2003).

Woolsack weathering (Pötzsch 1803), exhumed inselbergs, exfoliation domes (Gilbert 1904) and castle koppies are common surface features of the South Bohemian batholith (cf. Huber 1996, and references cited therein). Giant boulders and wobbling stones (so-called 'Wackelsteine') occur in the vicinity of Gmünd (Kieslinger 1964; Köhler 1976) and on many other granite exposures of the Waldviertel. The woolsacks result from blocky dissection by tension cracks (Cloos 1925) and sub-horizontal exfoliation (Gilbert 1904), and from subsequent hydrolysis of feldspar that starts at the joints, softens the rock and produces granular disintegration (Wilhelmy 1981). Strong hydrolysis mainly takes place in the zone of groundwater saturation, below the water table. Resulting deep weathering profiles of tropical peneplains can be tens or even hundreds of meters thick (Ollier 1988). It is generally assumed that such deep weathering and peneplanation of Variscan granite in central Europe has developed in a humid tropical climate (Borger 1992). Thus, the present-day weathering basal relief (Büdel 1957) should be inherited from Early Cenozoic (pre-Miocene) or even earlier times. Preservation of Mesozoic weathering profiles until present is indeed known from Australia (Ollier 1988). On the other hand, geomorphological investigations in the Aegean archipelago (Greece) have shown that peneplanation can proceed rather fast (within less than 10 Ma) when climatic conditions are appropriate (Riedl 2004).

Relict planation levels are widespread in the southern Bohemian Massif. Fischer (1979) interpreted them in terms of a peneplain staircase ('Rumpfflächentreppe') that corresponds to the concept of a piedmont staircase (Spreitzer 1951; cf. also Riedl 2007, and references cited therein). He distinguished four palaeoplanation levels that he ascribed to post-Cretaceous to pre-Eggenburgian piedmont steps. The Weinsberg peneplain staircase

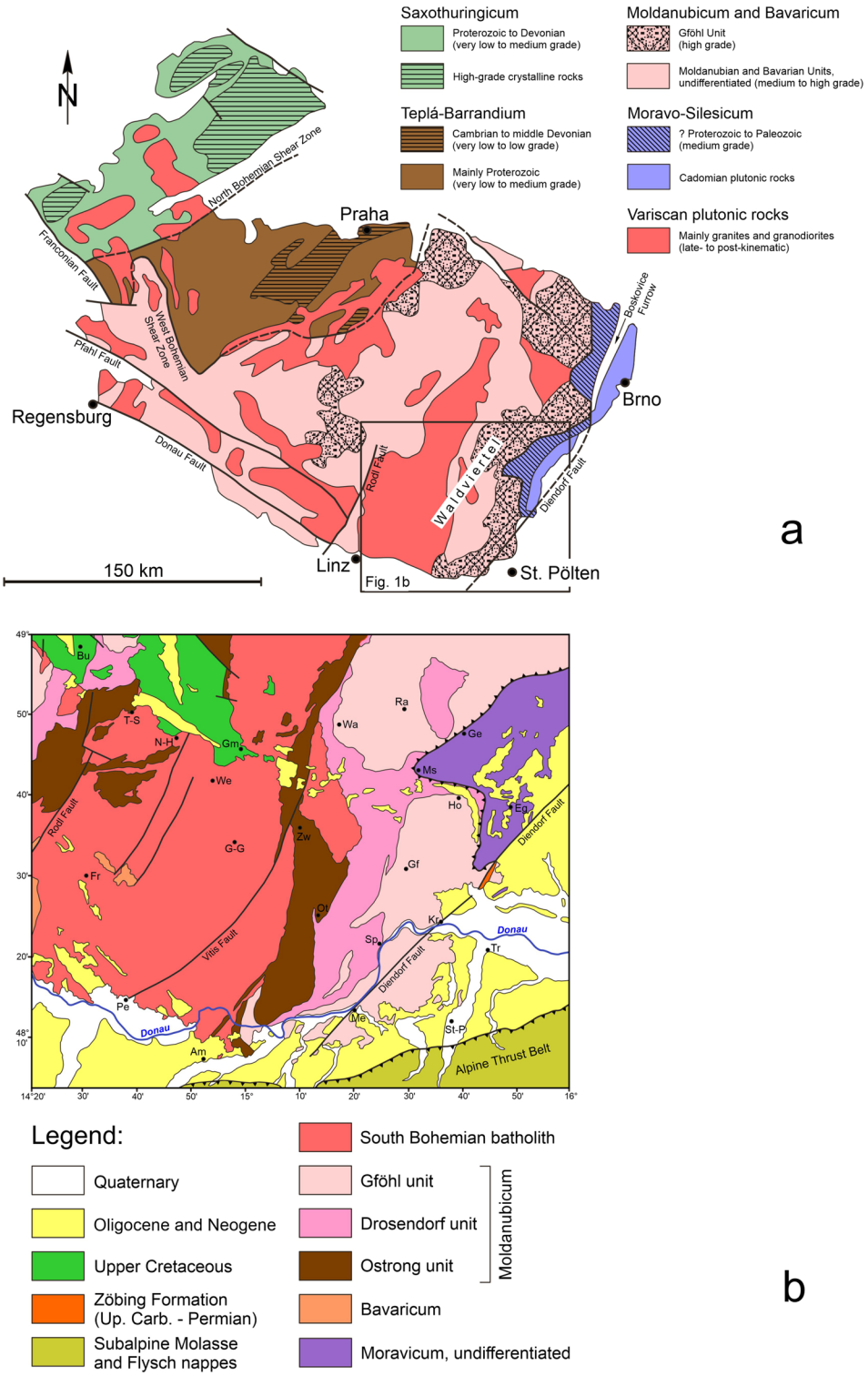

Fig. 1 Sketch map (**a**) of the southern and western Bohemian Massif (modified after Glasmacher et al. 2002) and **g**eological map (**b**) of the southeastern Bohemian Massif and its surroundings (simplified after Schnabel et al. 2002). *Am* Amstetten, *Bu* České Budějovice, *Eg* Eggenburg, *Fr* Freistadt, *Ge* Geras, Gf Gföhl, *G-G* Großgerungs, Gm Gmünd, *Ho* Horn, *Kr* Krems, *Me* Melk, *Ms* Messern, N-H Nové Hrady, *Ot* Ottenschlag, *Pe* Perg, *Ra* Raabs, *Sp* Spitz, *St-P* St. Pölten, *Tr* Traismauer, *T-S* Trhové Sviny, *Wa* Waidhofen a.d. Thaya, *We* Weitra, *Zw* Zwettl

('Rumpfflächentreppe im Weinsberger Wald') comprises the oldest planation relics on top of the Weinsberg Forest (> 940 m, 'Hochfläche von Bärnkopf'), and three lower planation levels which become progressively younger with decreasing altitude. These lower stages of peneplanation occur between 850 and 880 m, between 760 and 810 m, and between 720 and 750 m. These palaeoplanation levels are supposed to occur at quite similar altitudes on both sides of the NW–SE trending watershed of the Weinsberg Forest. Younger levels of pedimentation between 550 and 400 m altitude, in the vicinity of the river Danube (Donau) and its tributaries, are supposed to have a Neogene age.

Quaternary terraces of the Danube are located below 400 m altitude.

Two essential aspects of the geomorphological concept of Fischer (1979) should be born in mind. First, the NW–SE trending ridge of Weinsberg Forest is not a first-order continental watershed. The continental divide between the North Sea catchment (Vltava-Elbe) and the Black Sea catchment (Donau) is farther to the N, close to the national border between the Czech Republic and Austria. This continental divide is unspectacular from a geomorphological point of view. The Weinsberg Forest is even not a second-order watershed, like those between the catchments of major rivers as Rhine, Elbe or Oder. It just constitutes a local divide between the small rivers Krems and Kamp to the NE, and even smaller rivers to the SW (Gusen, Aist, Naarn, Isper, etc.). The horizontal distance between their headwater sources and their confluence into the Danube is less than 80 km. A second important fact is that the most spectacular giant woolsacks, mushroom rocks, wobbling stones and castle koppies do not occur on top of the Weinsberg Forest ('Zentrales Bergland' above 1000 m, and 'Hochfläche von Bärnkopf' at 940–980 m altitude) but farther to the N at altitudes below 600 m—especially in the nature park 'Blockheide Eibenstein' close to the town of Gmünd (Kieslinger 1964; Huber 1996).

Thermochronological methods

AFT dating and track length measurements

46 samples were collected from the South Bohemian batholith and from metamorphosed rocks of the Moldanubicum and the Moravo-Silesicum. Except for one paragneiss sample (BM 7), all samples originate from plutonic rocks or metamorphosed plutonic rocks. Locations and rock types are indicated in Supplement file 1. For a better comparison with the already published dataset of Hejl et al. (2003), we have merged the 19 old and the 27 new samples in common tables (Tables 1, 2, and 3) and in Fig. 2.

After crushing and dry sieving, the fractions with grain sizes between 100 and 250 µm were chosen for mineral separation. Apatite was enriched by chemical flotation (Hejl and Ney 1994), by magnetic and heavy liquid separation.

The grain-population method (cf. Gleadow 1981; Wagner and Van den haute 1992) was applied for dating, because it is well suitable for apatite with fairly homogeneous uranium concentrations, as it can be assumed for apatite of magmatic origin. An aliquot of each apatite concentrate was heated for 24 h at 550 °C in a muffle furnace and then irradiated with thermal neutrons. Samples BM 47 to BM 58 were irradiated in channel 8 of the Thetis nuclear reactor at the University of Ghent (Belgium). The other samples were irradiated in the Astra reactor of the Forschungszentrum Seibersdorf (Austria). Both irradiation facilities had a good thermalization. Thermal neutron fluences were between 3.7×10^{14} and 2.2×10^{15} cm^{-2} (Table 1), and the epithermal neutron flux amounted to less than 0.1% of the total flux. Thermal neutron fluences were determined by γ-spectrometry of activated Co and Au monitors (Van den haute et al. 1988). Natural and irradiated grains of each sample were embedded separately in epoxy resin, ground, polished and etched with 5% HNO_3 for 60 s at 20 °C. The ^{238}U spontaneous fission decay constant $\lambda_f = 8.46 \times 10^{-7}$ a^{-1} (Galliker et al. 1970) was used for age calculations. System calibration was repeatedly tested with Durango apatite (Jonckheere et al. 1993, 2015) and apatite from Mt. Dromedary banatite (Green 1985). Dating results are reported in Table 1.

Polished apatite mounts of 27 unirradiated samples with spontaneous track densities above 7×10^5 cm^{-2} were overetched with an aqueous solution of 5.5 M HNO_3 for 20 s at 21 °C, and then examined for fully confined, horizontal tracks (Gleadow et al. 1986a, b). Length measurements were performed with a drawing tube attachment to the microscope and a digitizing tablet (cf. Wagner and Van den haute 1992). Individual track length measurements were performed with a precision of ± 0.2 µm. Results of confined track lengths measurements—including mean lengths, standard deviations and Dpar—are reported in Table 2. Frequency distributions (histogram classes) are reported in Table 3. A mean induced track length of 16.2 µm was determined on a sample of irradiated Durango apatite age standard (Jonckheere et al. 1993, 2015). This value is similar to that reported by Gleadow et al. (1986b).

Apatite (U–Th)/He dating

AHe analysis was conducted on a subset of samples that had been previously dated with AFT. Three samples (BM 1, 5, 11) were analyzed at the University of Göttingen (Germany). Five samples (BM 14, 40, 43, 46, 54) were dated at Dalhousie University (Canada). Results are given in Tables 4 and 5. For a detailed description of AHe dating, the reader is referred to a recent extensive review in Flowers et al. (2022a, b). Details on the analytical procedure of Göttingen and Dalhouse laboratories are provided in supplementary file 2. Here, only a brief outline is given.

AHe thermochronology is based on the production of α-particles (i.e., He atoms) during radioactive decay of ^{238}U, ^{235}U, ^{232}Th and ^{147}Sm. Retention of these ^4He nuclides within the crystal lattice versus their loss by diffusion is temperature dependent and closure temperatures may range between ~ 40 and ~115 °C.

He diffusivity is impacted by various factors, among which radiation damage (e.g., Shuster et al. 2006; Flowers et al. 2009; Gautheron et al. 2009), and grain size (e.g.,

Table 1 Results of apatite fission-track (AFT) age determinations

Sample code	Analyst	No. of grains	Spontaneous tracks		Induced tracks		ρ_s/ρ_i	Error 1σ	Neutron fluence	Fission-track
		(n_s/n_i)	N_s	ρ_s (10^5 cm^{-2})	N_i	ρ_i (10^5 cm^{-2})		of ρ_s/ρ_i (%)	(10^{14} cm^{-2})	age $\pm 1\sigma$ (Ma)
GFO 5	EH	300/500	1691	3.52	435	0.54	6.48	7.97	3.76	120.1 ± 10
BIT 1	EH	200/400	2394	7.48	377	0.59	12.70	9.73	3.76	233.3 ± 23.4
SPI 1	EH	300/500	2045	11.83	602	2.09	5.66	5.73	3.76	105 ± 6.6
FR 13–91	EH	200/300	506	1.58	107	0.22	7.09	11.44	3.76	131.3 ± 15.4
EGG 1	EH	50/150	741	9.26	236	0.98	9.42	11.96	3.76	173 ± 21.2
FR 21–91	EH	50/100	541	6.76	103	0.64	10.50	15.55	3.76	193.5 ± 30.5
GRA 1	EH	150/300	714	8.26	200	1.16	8.26	11.23	3.76	132.2 ± 15.2
BM 1	GS	70/70	1078	26.73	1053	26.12	1.02	6.39	21.80	104.8 ± 6.2
	EH	50/50	463	16.08	534	18.54	0.87	9.59		
BM 2	GS	70/70	313	7.76	358	8.88	0.87	18.83	21.80	91.9 ± 13.5
	EH	70/70	590	5.27	707	6.31	0.83	22.45		
BM 3	GS	70/70	1006	24.95	1082	26.84	0.93	5.06	21.80	98.5 ± 5
	EH	50/50	527	18.30	597	20.71	0.88	9.08		
BM 4	GS	70/70	951	23.59	983	24.38	0.97	9.34	21.80	104 ± 7.6
	EH	70/70	601	14.91	622	15.43	0.97	9.99		
BM 5	GS	70/70	830	20.59	721	17.88	1.15	6.23	21.80	122.2 ± 7
	EH	50/50	455	15.80	409	14.20	1.11	9.25		
BM 6	GS	82/82	912	19.31	744	15.75	1.23	9.94	21.80	130.3 ± 10.5
	EH	70/70	569	14.11	480	11.90	1.19	11.92		
BM 7	GS	100/100	1578	27.40	1398	24.27	1.13	7.33	21.40	119.3 ± 7.1
	EH	50/50	575	19.97	507	17.60	1.13	7.89		
BM 8	GS	70/70	545	13.52	472	11.71	1.15	8.38	21.40	114.9 ± 7.6
	EH	70/70	445	11.04	436	10.81	1.02	8.91		
BM 9	GS	50/50	387	13.44	261	9.06	1.48	11.32	21.40	145.7 ± 10.5
	EH	70/70	485	12.03	368	9.13	1.32	9.30		
BM 10	GS	70/70	279	6.92	253	6.27	1.10	12.47	21.40	109.2 ± 10.6
	EH	62/62	239	6.69	251	7.03	0.95	14.23		
BM 11	GS	150/150	475	5.50	308	3.56	1.54	9.80	21.40	171.5 ± 13.8
	EH	150/150	370	4.28	208	2.41	1.78	12.35		
BM 12	GS	100/150	423	2.64	331	1.38	2.24	14.10	21.40	216.3 ± 21.3
	EH	70/100	286	2.55	182	1.14	1.92	12.96		
BM 14	EH	100/100	1148	19.93	1029	17.86	1.12	6.73	21.70	119.3 ± 8.6
BM 15	EH	60/60	561	16.23	462	13.37	1.21	11.99	21.70	129.8 ± 15.9
BM 16	EH	50/50	657	22.81	516	17.92	1.27	8.51	21.70	136 ± 12.1
BM 17	EH	150/150	791	9.16	781	9.04	1.01	7.95	21.70	108.4 ± 9
BM 20	EH	200/200	766	6.65	641	5.56	1.20	8.65	21.70	127.7 ± 11.5
BM 21	EH	200/200	352	3.06	238	2.07	1.47	12.81	21.70	157.7 ± 20.6
BM 36	GS	100/100	2152	37.36	2713	47.10	0.79	4.35	18.10	71 ± 3.4
BM 37	GS	100/100	324	5.63	398	6.91	0.81	11.39	17.40	70.1 ± 8.1
BM 38	GS	35/35	217	10.76	237	11.76	0.92	16.10	18.90	85.5 ± 13.9
BM 39	GS	100/100	237	4.11	263	4.57	0.90	14.28	18.00	80.2 ± 11.6
BM 40	GS	100/100	1317	22.86	974	16.91	1.35	4.77	17.50	116.6 ± 6
BM 41	GS	100/100	382	6.63	459	7.97	0.83	8.63	18.50	76.1 ± 6.8
BM 42	GS	50/50	459	15.94	419	14.55	1.10	12.80	19.40	104.9 ± 13.6
BM 43	GS	100/100	535	9.29	814	14.13	0.66	7.74	18.50	60.2 ± 4.8
BM 44	GS	100/100	348	6.04	488	8.47	0.71	9.23	18.50	65.3 ± 6.2
BM 45	GS	100/100	505	8.77	772	13.40	0.65	9.05	18.80	60.9 ± 5.6
BM 46	GS	100/100	316	5.49	428	7.43	0.74	9.16	18.50	67.6 ± 6.3

Table 1 (continued)

Sample code	Analyst	No. of grains	Spontaneous tracks		Induced tracks		ρ_s/ρ_i	Error 1σ	Neutron fluence	Fission-track
		(n_s/n_i)	N_s	ρ_s (10^5 cm^{-2})	N_i	ρ_i (10^5 cm^{-2})		of ρ_s/ρ_i (%)	(10^{14} cm^{-2})	age ± 1σ (Ma)
BM 47	GS	50/50	641	22.26	140	4.86	4.58	11.66	10.39	232.4 ± 27.7
BM 48	GS	50/50	843	29.27	221	7.67	3.81	9.66	10.47	195.7 ± 19.5
BM 49	GS	100/100	629	10.92	139	2.41	4.53	10.91	10.71	236.7 ± 26.5
BM 50	GS	100/100	221	3.84	71	1.23	3.11	14.31	11.17	170.7 ± 24.8
BM 51	GS	100/100	413	7.17	160	2.78	2.58	11.73	11.18	142 ± 17
BM 53	GS	50/50	921	31.98	203	7.05	4.54	18.18	11.34	251 ± 46.1
BM 54	GS	100/100	328	5.69	74	1.28	4.43	13.89	10.82	234.2 ± 33.1
BM 55	GS	100/100	330	5.73	137	2.38	2.41	13.63	10.59	125.7 ± 17.4
BM 57	GS	100/100	757	13.14	188	3.26	4.03	9.88	11.04	217.4 ± 22.2
BM 58	GS	100/100	507	8.80	127	2.20	3.99	9.86	10.80	211 ± 21.5

Analysts: Ewald Hejl (EH) and Gert Sekyra (GS). The age is given as an error-weighted average for those samples that have been counted by both analysts. N_s, N_i, total number of counted tracks (spontaneous and induced, respectively); ρ_s, ρ_i, areal track densities (spontaneous and induced, respectively)

Table 2 Synopsis of AFT ages, confined track length data and Dpar

Sample code	Fission-track age ± 1σ (Ma)	Track length data			Dpar (μm)
		n	l (μm)	s (μm)	
BIT 1	233.3 ± 23.4	60	13.18	1.51	1.70
SPI 1	105 ± 6.6	60	13.11	1.57	1.90
GRA 1	132.2 ± 15.2	50	12.29	1.92	1.70
BM 1	104.8 ± 6.2	100	13.06	1.75	2.07
BM 4	104 ± 7.6	80	12.92	1.82	1.71
BM 5	122.2 ± 7	80	12.38	1.80	1.94
BM 6	130.3 ± 10.5	100	12.94	1.95	1.97
BM 7	119.3 ± 7.1	80	13.08	1.91	2.23
BM 8	114.9 ± 7.6	80	13.40	1.86	1.98
BM 9	145.7 ± 10.5	60	12.88	1.86	2.16
BM 14	119.3 ± 8.6	80	12.3	1.85	2.38
BM 15	129.8 ± 15.9	40	13.31	1.97	2.95
BM 16	136 ± 12.1	45	13.19	1.61	3.33
BM 17	108.4 ± 9	28	12.92	2.04	2.51
BM 36	71 ± 3.4	80	12.71	1.38	1.92
BM 38	85.5 ± 13.9	22	12.74	2.07	1.90
BM 40	116.6 ± 6	70	11.99	1.89	1.96
BM 42	104.9 ± 13.6	50	12.76	1.88	2.00
BM 43	60.2 ± 4.8	40	12.10	1.95	2.01
BM 45	60.9 ± 5.6	40	12.65	1.84	2.46
BM 47	232.4 ± 27.7	60	12.54	1.93	2.10
BM 48	195.7 ± 19.5	60	12.72	1.75	2.05
BM 49	236.7 ± 26.5	55	13.18	1.71	2.53
BM 51	142 ± 17	30	13.25	1.95	1.93
BM 53	251 ± 46.1	80	12.29	1.75	2.03
BM 57	217.4 ± 22.2	60	12.13	1.65	2.05
BM 58	211 ± 21.5	60	12.81	1.53	1.86

n number of measured track lengths, l arithmetic mean, s standard deviation (1σ)

Farley 2000) are considered as the most important ones. Grain size determines how much He nuclei are ejected from the crystal, since the α-particle travels through the grain upon its generation (the alpha stopping distance in apatite is on average 18 μm, Flowers et al. (2022a). He atoms produced by parent nuclides that are located in the proximity of the crystal's rim are more likely to get ejected. Therefore, AHe ages are generally corrected for He loss using a geometric correction factor (Ft), which takes the size and the shape of each dated crystal into account (Farley et al. 1996).

The kinetic differences in He diffusion between individual grains are particularly important for samples experiencing protracted cooling, i.e., with a sufficiently long residence time in the He partial retention zone to induce partial diffusive He loss. For datasets with high intra-sample dispersion, such as the one presented within this study, single-grain ages are plotted vs. equivalent spherical radii (ESR; proxy for grain size) and effective uranium (eU; proxy for radiation damage calculated as $eU = U + 0.235 \cdot Th + 0.0046 \cdot Sm$). If correlations are observed, even highly dispersed datasets can enhance thermal history models, as kinetic models incorporate He diffusion as a function of damage accumulation and annealing (e.g.,Flowers et al. 2009; Gautheron et al. 2009). If no such correlation exists, we here follow the approach of not including AHe data into the interpretive process of thermal history modeling and only report the dataset. We define a threshold level of 20% dispersion, below which we calculate and report an unweighted mean age and the standard deviation. Following these criteria, it turned out that only one sample remained to be integrated into thermal history modeling implementing the RDAAM annealing code of Flowers et al. (2009).

Table 3 Frequency distributions of confined track lengths (tracks per histogram class and corresponding percentages)

Sample	Sum	Histogram classes (µm)/tracks per class (above)/% per class (below)										
code	*n*/%	7–8	8–9	9–10	10–11	11–12	12–13	13–14	14–15	15–16	16–17	17–18
BIT 1	60	0	0	0	6	7	12	17	11	6	1	0
	100.00	0.00	0.00	0.00	10.00	11.67	20.00	28.33	18.33	10.00	1.67	0.00
SPI 1	60	0	1	0	7	6	8	21	11	4	2	0
	100.00	0.00	1.67	0.00	11.67	10.00	13.33	35.00	18.33	6.67	3.33	0.00
GRA 1	50	1	2	6	3	5	12	12	8	1	0	0
	100.00	2.00	4.00	12.00	6.00	10.00	24.00	24.00	16.00	2.00	0.00	0.00
BM 1	100	1	2	3	8	13	14	27	23	8	1	0
	100.00	1.00	2.00	3.00	8.00	13.00	14.00	27.00	23.00	8.00	1.00	0.00
BM 4	80	2	0	4	6	8	17	19	17	6	1	0
	100.00	2.50	0.00	5.00	7.50	10.00	21.25	23.75	21.25	7.50	1.25	0.00
BM 5	80	0	6	4	7	17	10	20	15	1	0	0
	100.00	0.00	7.50	5.00	8.75	21.25	12.50	25.00	18.75	1.25	0.00	0.00
BM 6	100	0	6	5	9	7	10	30	22	9	2	0
	100.00	0.00	6.00	5.00	9.00	7.00	10.00	30.00	22.00	9.00	2.00	0.00
BM 7	80	1	1	5	9	5	9	19	17	14	0	0
	100.00	1.25	1.25	6.25	11.25	6.25	11.25	23.75	21.25	17.50	0.00	0.00
BM 8	80	0	1	6	5	3	12	18	19	14	2	0
	100.00	0.00	1.25	7.50	6.25	3.75	15.00	22.50	23.75	17.50	2.50	0.00
BM 9	60	0	2	5	2	10	11	13	10	5	2	0
	100.00	0.00	3.33	8.33	3.33	16.67	18.33	21.67	16.67	8.33	3.33	0.00
BM 14	80	0	1	10	9	14	15	15	9	6	1	0
	100.00	0.00	1.25	12.50	11.25	17.50	18.75	18.75	11.25	7.50	1.25	0.00
BM 15	40	0	1	1	3	4	6	9	7	5	4	0
	100.00	0.00	2.50	2.50	7.50	10.00	15.00	22.50	17.50	12.50	10.00	0.00
BM 16	45	0	0	0	3	7	10	8	10	6	1	0
	100.00	0.00	0.00	0.00	6.67	15.56	22.22	17.78	22.22	13.33	2.22	0.00
BM 17	28	0	1	2	2	3	4	6	6	3	1	0
	100.00	0.00	3.57	7.14	7.14	10.71	14.29	21.43	21.43	10.71	3.57	0.00
BM 36	80	0	1	7	6	8	25	20	10	2	1	0
	100.00	0.00	1.25	8.75	7.50	10.00	31.25	25.00	12.50	2.50	1.25	0.00
BM 38	22	0	2	1	2	1	3	4	8	1	0	0
	100.00	0.00	9.09	4.55	9.09	4.55	13.64	18.18	36.36	4.55	0.00	0.00
BM 40	70	0	3	6	15	11	10	14	6	5	0	0
	100.00	0.00	4.29	8.57	21.43	15.71	14.29	20.00	8.57	7.14	0.00	0.00
BM 42	50	1	0	2	4	12	4	13	8	4	2	0
	100.00	2.00	0.00	4.00	8.00	24.00	8.00	26.00	16.00	8.00	4.00	0.00
BM 43	40	0	5	2	3	5	9	10	4	2	0	0
	100.00	0.00	12.50	5.00	7.50	12.50	22.50	25.00	10.00	5.00	0.00	0.00
BM 45	40	1	0	1	5	6	11	5	7	2	2	0
	100.00	2.50	0.00	2.50	12.50	15.00	27.50	12.50	17.50	5.00	5.00	0.00
BM 47	60	2	1	3	6	6	18	7	12	4	1	0
	100.00	3.33	1.67	5.00	10.00	10.00	30.00	11.67	20.00	6.67	1.67	0.00
BM 48	60	0	2	2	2	12	15	11	10	4	2	0
	100.00	0.00	3.33	3.33	3.33	20.00	25.00	18.33	16.67	6.67	3.33	0.00
BM 49	55	0	0	1	3	13	5	13	10	7	3	0
	100.00	0.00	0.00	1.82	5.45	23.64	9.09	23.64	18.18	12.73	5.45	0.00
BM 51	30	0	0	3	1	4	1	7	8	5	1	0
	100.00	0.00	0.00	10.00	3.33	13.33	3.33	23.33	26.67	16.67	3.33	0.00
BM 53	80	2	1	5	7	16	21	16	7	4	1	0

Table 3 (continued)

Sample	Sum	Histogram classes (µm)/tracks per class (above)/% per class (below)										
code	*n*/%	7–8	8–9	9–10	10–11	11–12	12–13	13–14	14–15	15–16	16–17	17–18
	100.00	2.50	1.25	6.25	8.75	20.00	26.25	20.00	8.75	5.00	1.25	0.00
BM 57	60	0	2	4	5	16	13	12	6	1	1	0
	100.00	0.00	3.33	6.67	8.33	26.67	21.67	20.00	10.00	1.67	1.67	0.00
BM 58	60	0	1	1	5	7	16	15	10	5	0	0
	100.00	0.00	1.67	1.67	8.33	11.67	26.67	25.00	16.67	8.33	0.00	0.00

Thermochronological results

Regional pattern and frequency distribution of measured AFT ages

The AFT ages range from 251 ± 46 Ma (Latest Permian) to 60.2 ± 4.8 Ma (Paleocene). We observe a decrease of measured ages from NE to SW, but no significant age breaks (i.e., exceeding the error limits) at the Late Variscan Vitis and Diendorf faults (Fig. 2). Thus, strong vertical offset (> ca. 500 m) on these is precluded for Cretaceous and Cenozoic times. This has already been stated by Hejl et al. (2003).

The highest AFT age was that of sample BM 53 which originates from a Gföhl gneiss between the towns of Horn and Gföhl. Seven other AFT ages above 200 Ma were measured for surrounding locations (BM 12, 47 and 54) and for the area farther to the N (BIT 1, BM 49, 57 and 58). The samples of this highest age group originate from Gföhl gneiss (3 samples), granulite (2 samples), Dobra gneiss (1 sample) and Bittesch gneiss (2 samples). No age break occurs at the thrust front of the Moldanubian onto the Moravian units. Within the area with highest AFT ages (> 200 Ma), also lower ages were measured. The lowest age of this area was found for sample BM 10 (109.2 ± 10.6 Ma). Because of the small variation in sampling altitudes (from 280 to 551 m) compared to the much larger horizontal distances between sampling locations (up to ca. 40 km), a plot of AFT ages versus altitude has not been made because it could be misleading for the area under discussion.

A quite homogeneous group of Early Cretaceous AFT ages (between 142 ± 17 and 104 ± 7.6 Ma) dominates the summit region and the northeastern slopes of the Weinsberg Forest, down to the Kamp valley (Fig. 2) to the E of the town of Zwettl. Two samples to the W and S of the town of Groß-Gerungs (BM 2 and 3) yielded slightly lower AFT ages of 91.9 ± 13.5 Ma and 98.5 ± 5 Ma, respectively (Fig. 2). Thus, the whole area exhibits only moderate age variations over a horizontal distance of ca. 60 km from NW to SE.

Distinctly lower AFT ages were measured for the samples from the SW of the Weinsberg Forest, i.e., from an elevation of 750 m (BM 39) down to the slopes of the river Danube at ca. 300 m altitude (BM 43). Ages of this group range from 104.9 ± 13.6 Ma to 60.2 ± 4.8 Ma (Middle Cretaceous to Paleocene). They are significantly lower than the AFT ages of the samples from similar elevation on the northeastern side of the Weinsberg Forest.

The measured AFT ages exhibit an Early Cretaceous frequency maximum between ca. 145 and 100 Ma (Fig. 3). Most AFT ages of samples from the northeastern slopes of the Weinsberg Forest belong to this group.

AFT length data

Frequency distributions of confined track lengths (Gleadow et al. 1986a, b) as well as corresponding mean track lengths and standard deviations were determined for 27 samples (Figs. 4, 5, 6 and 7). Only those samples with at least 80 confined track lengths measurements were chosen for thermochronological modeling. To facilitate their interpretation, the histograms are grouped according to the AFT age classes of Figs. 2, 3 and 4 (i.e. > 200 Ma; 200–145 Ma; 145–100 Ma; < 100 Ma).

Arithmetic means of all length distributions range between 11.99 µm and 13.40 µm. According to Gleadow et al. (1986b), values around 12 µm or 13 µm are typical for basement terrains, which have never been significantly disturbed thermally since their original magmatic emplacement or metamorphism. Standard deviations of all length distributions range from 1.38 to 2.07 µm.

Apatite (U–Th)/He results

All analyzed samples delivered inclusion-free, fracture-free, euhedral grains of sufficient size with sphere radii well above 50 µm. For the Göttingen sample subset, 3–4 grains per sample were measured (Table 4), for the Dalhousie sample subset 5 crystals per sample were measured (Table 5). Intra-sample data variation is high for almost all samples with individual dates ranging from 25 ± 0.1 to 525 ± 42 Ma and dispersion varying from 16 to 64%. Supplementary file 3 displays age-eU and size-eU plots for all samples. Since we neither find a positive correlation between age and eU nor between age and grain size, we cannot pinpoint the first-order kinetic controls for date dispersion and thus refrain from including these samples into thermal history modeling. We report a mean age for sample BM 5, since its dispersion

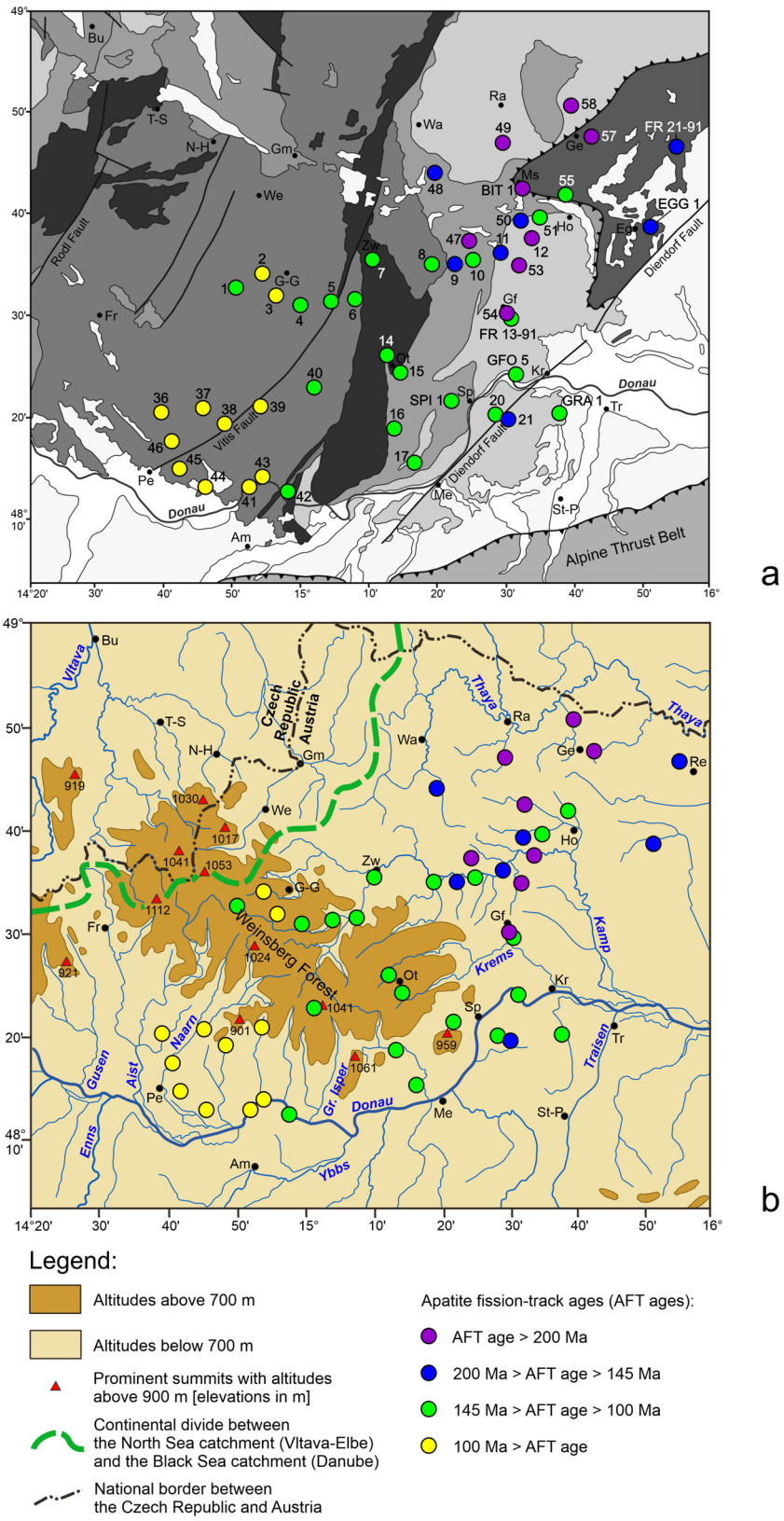

Fig. 2 Regional distribution of AFT samples and age groups (**a**) and topographical sketch map with fluvial drainage pattern, selected summits and regional distribution of AFT age groups (**b**)

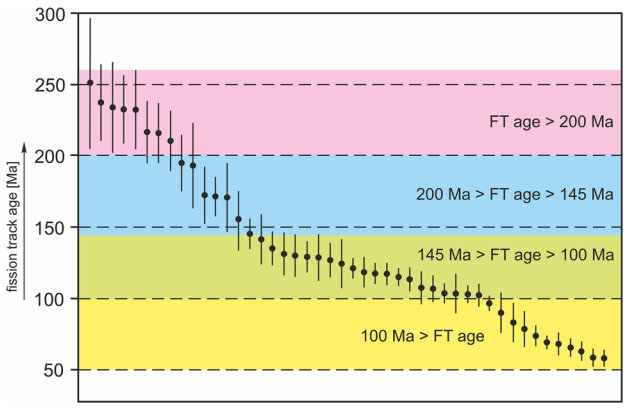

Fig. 3 Frequency distribution of measured AFT ages, i.e., in descending order of measured ages with 1σ error bars

is 16% only. The AHe mean age of 110 ± 18 Ma is younger than the AFT age of 122 ± 7 Ma. There is no standard protocol on when and how to combine individual dates, but we here apply a threshold of 20%. In the absence of positive relationships, He implantation or uncharacterized eU zonation may be responsible for data scatter, since He ejection correction assumes a homogeneous distribution of the parent nuclides. However, our AFT analysis revealed very little internal zoning.

Mesozoic and Cenozoic palaeogeography

For a better understanding of the central European paleogeography, we have added the sketch maps of Fig. 8, which roughly display the regional extent of mainland, marine and coastal areas for selected periods of the Mesozoic and Cenozoic. These sketch maps were compiled after Ziegler (1990), Faupl (1997) and Park (2014).

In the following, we briefly outline the waxing and waning of seas in our study area as derived from the sedimentary record. Since discordant sedimentary horizons pin surface (re-) exhumation of basement rocks, they serve as first-order constraints for thermal modeling of thermochronology data, as will be explained in the next chapter.

Sediments of the Boskovice furrow in Moravia (Fig. 1a) are of Late Carboniferous to Permian age. Similar sediments occur farther south at the village of Zöbing, where a tectonically isolated block of arkoses, sand-, and siltstones is squeezed between two segments of the Diendorf fault (cf. Fig. 1b). The Late Carboniferous to Early Permian Zöbing formation has a thickness of ca. 1000 m (Vasicek 1991). This isolated occurrence of thick pre-Mesozoic sediments demonstrates that late-Variscan exhumation of basement rocks was not regionally uniform, but was complicated by a mosaic of mountain ranges and intermontane basins (Fazlikhani et al. 2022; Ziegler 1990).

In Triassic times, the Bohemian Massif was part of the Vindelicic-Bohemian mainland, which separated the shallow-marine, epicontinental German basin from the northern Tethys (Fig. 8a). Coastal fans, fluvial and lacustrine sedimentation were restricted to the western margin of the Bohemian Massif (Schröder et al. 1997), while most parts of the regions farther east were mainland.

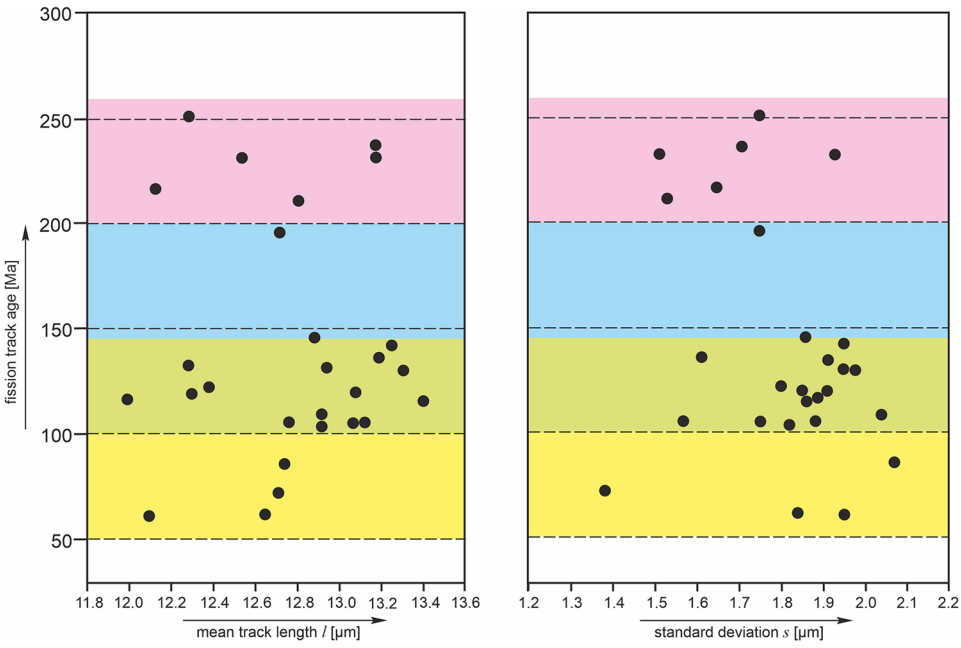

Fig. 4 Confined track lengths data versus AFT ages. **a** Mean track length vs. AFT age; **b** standard deviation vs. AFT age. Background colors visualize the same age intervals as in Fig. 4

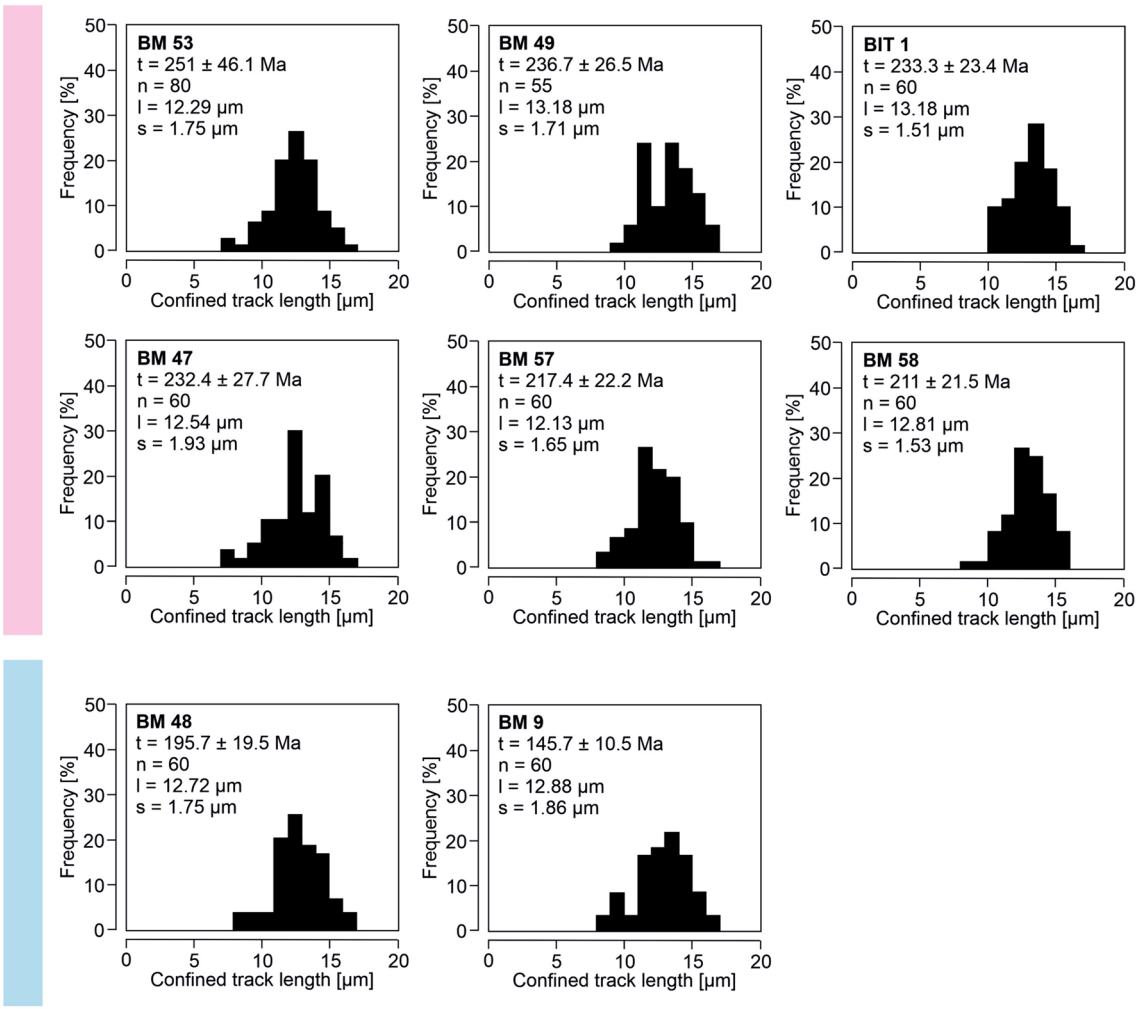

Fig. 5 Frequency distributions of confined spontaneous track lengths in apatite for samples with Triassic and Jurassic AFT ages. Colored bars on the left side correspond to the colors indicating the age intervals in Figs. 3 and 4

A Jurassic transgression of the northern Tethys inundated the southern shore of the Vindelicic-Bohemian mainland and culminated in Late Jurassic time. Marginal parts of the Bohemian Massif became submerged, and a marine channel separated its major part from a Sudetic island in the N (Fig. 8b). The preserved thickness of Jurassic formations in the area of the later North Alpine molasse zone locally exceeds 500 m (Malzer et al. 1993). Significant reburial of the southeastern Bohemian Massif by Late Jurassic sediments may have occurred too, because gravels of cherty limestones of presumable Late Jurassic age were found in Neogene sediments to the NE of the town of Krems (Steininger and Roetzel 1996). However, position and shape of the Late Jurassic shoreline are unknown.

Because of a strong regression at the end of the Jurassic, many regions of western and central Europe became part of a large mainland. In the Early Cretaceous at ca. 130 Ma, it included the Brabant Massif, middle and northern Germany, Bohemia and Moravia (Fig. 8c). Limnic and brackish sedimentation—including coal measures—occurred along the coast, while central parts of the mainland were subjected to erosion under a humid tropical climate (cf. Ziegler 1990; Faupl 1997). This period of intensive tropical weathering on a broadly emerged mainland temporally coincides with the frequency maximum of AFT ages between ca. 145 and 100 Ma that we interpret as cooling ages produced by strong erosion and continuous cooling through the entire partial annealing zone (PAZ) for apatite fission tracks.

Extensive transgressions occurred during the Middle Cretaceous (Niebuhr et al. 2009). Major parts of the former mainland became progressively inundated. The sea-level rise culminated about 75 Ma ago, when southern Bohemia and the Rhenish Massif were still connected as a narrow elongated island (Fig. 8d). Several hundred meters of Late Cretaceous marine sediments accumulated in central and northern Bohemia (Ulčný 2001; Ulčný et al. 2009), as well

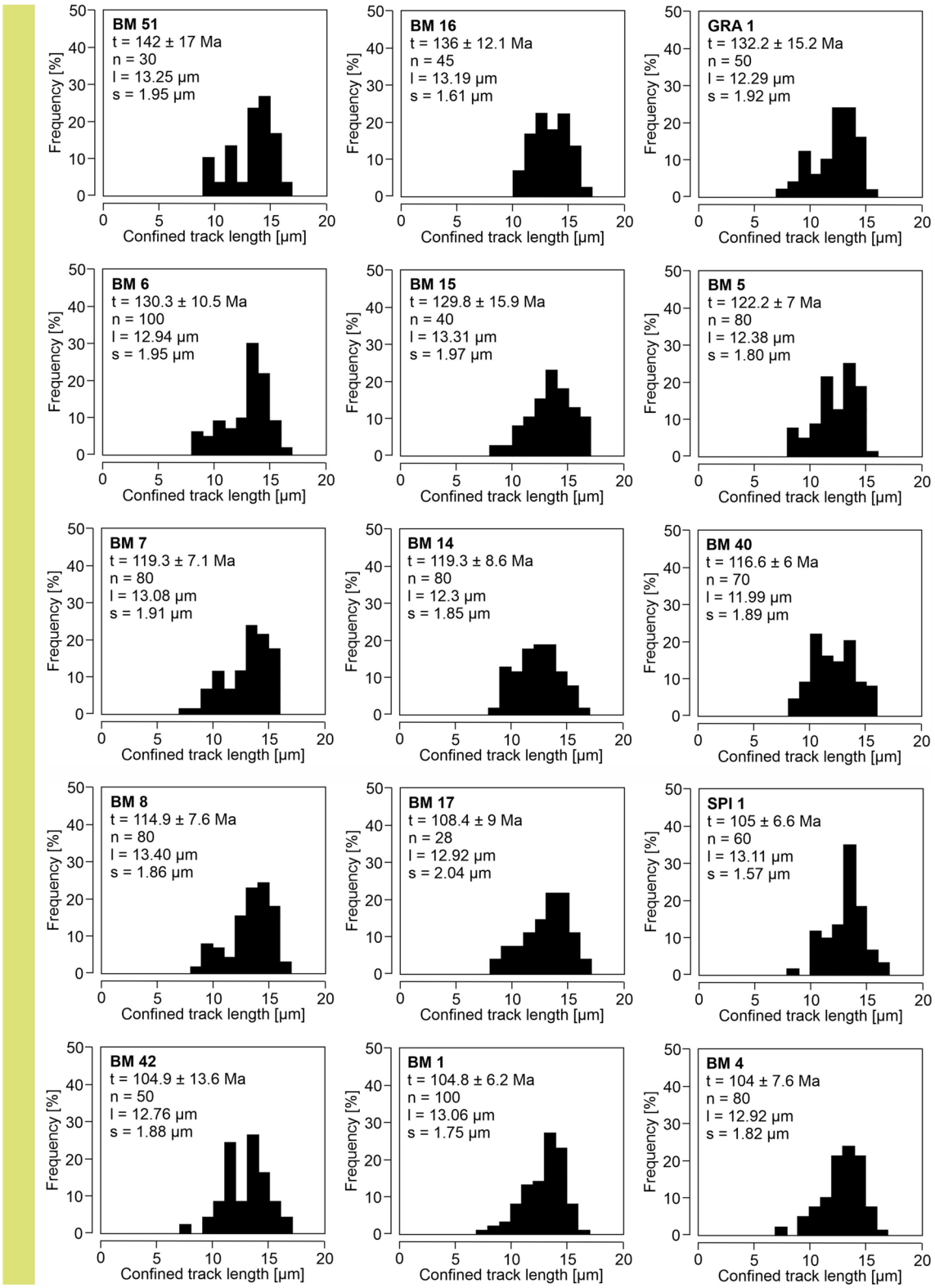

Fig. 6 Frequency distributions of confined spontaneous track lengths in apatite for samples with Early Cretaceous AFT ages. The green bar on the left side corresponds to the green color indicating the Early Cretaceous age interval in Figs. 3 and 4

as in the shelf area of the later North Alpine Molasse Zone (Malzer et al. 1993). The sedimentary basins of Třebon and Česke Budejovice to the NW of the town of Gmünd contain non-marine Late Cretaceous sediments with a thickness of 450 m (Suk 1984). Spectacular giant woolsacks of the nature park 'Blockheide Eibenstein' are located directly at the sedimentary base of Late Cretaceous sediments. Thus, they may belong to a 'sealed relief', i.e., a tropical weathering basal relief that could have developed during the Early Cretaceous and afterward was protected from further erosion by a thick cover of Late Cretaceous sediments. Such Late Cretaceous reburial has probably affected major parts of the Waldviertel (Hejl et al. 2003).

Paleocene and Eocene sediments are unknown from the Waldviertel. Most likely, the whole region was emerged und subjected to erosion (Roetzel and Steininger 1996). A Late Eocene transgression occurred farther south. Corresponding shallow marine and adjacent deltaic sediments of up to 120 m thickness are known from boreholes in the Upper Austrian molasses basin (Malzer et al. 1993). The shoreline of a Late Eocene sea was close to the southern margin of the present-day outcropping basement (Fig. 8e).

Strong subsidence of the North Alpine molasses basin started in Oligocene time, after the closure of the North Penninic Ocean. Consequently, the sea advanced toward the N and the shoreline touched the present-day border of the outcropping Variscan basement in Upper and Lower Austria (cf. Kuhlemann and Kempf 2002). Coastal sands of the Linz and Melk formations lie directly on top of the Variscan basement. They comprise brackish to shallow-marine sands and clays, as well as coal-bearing freshwater deposits (Malzer et al. 1993). Fluvial and lacustrine sediments of Oligocene age are even preserved deep inside the Waldviertel basement area. These silty sands, gravels and clays of the St. Marein-Freischling formation (cf. Roetzel and Steininger 1996) occur between the towns of Gmünd and Horn, in close vicinity to the headwaters of the Thaya and Kamp rivers. These sediments temporally constrain emergence of the basement units, but due to their limited thickness of less than 40 m (cf. Tollmann 1985), deep reburial is ruled out.

Few Badenian and Sarmatian marine to brackish sediments are preserved in the vicinity of the town of Krems, but in general, the Miocene sea did not submerge the present-day basement area and no transgressions occurred after the Sarmatian (Steininger and Roetzel 1996). Ongoing uplift since the Pannonian (about 10 Ma ago) created an eastward-orientated fluvial drainage of a Palaeo-Danube from Upper Austria to the Vienna basin (Unger 1989; Gyurits and Kurzweil 1976). A general drainage of the North Alpine Molasse Zone (including southern Germany) from W to E was established during the Late Pannonian or at the beginning of the Pliocene, i.e., about 7–5 Ma ago (Unger 1989).

Table 4 (U–Th)/He data from Göttingen University (Germany)

Sample	He			U			Th				Sm			Ejection	Uncorr	Ft-Corr		Sample unweighted			Dispersion (1σ/mean age) (%)	Range (given if dispersion > 20%)
	Vol	1σ		Mass	1 s	conc	Mass	1σ	Conc	Th/U	Mass	1σ	Conc	correct	He-age	He-age	2σ	Aver. ± 1 s.e. /		1σ		
	(ncc)	(%)		(ng)	(%)	(ppm)	(ng)	(%)	(ppm)	ratio	(ng)	(%)	(ppm)	(Ft)	(Ma)	(Ma)	(Ma)	(Ma)	(Ma)	(Ma)		
BM_1_a1	**7.053**	0.9		**0.477**	1.8	54	**0.044**	2.5	5	0.09	**2.913**	3.1	332	0.780	*113.3*	**145.4**	11.0					
BM_1_a2	**4.081**	0.9		**0.420**	1.8	48	**0.034**	2.5	4	0.08	**2.989**	3.1	340	0.833	*74.3*	**89.2**	5.6					
BM_1_a3	**5.953**	0.9		**0.245**	1.8	50	**0.025**	3.7	5	0.10	**1.851**	3.1	376	0.737	*182.8*	**247.9**	21.6					
BM_1_a4	**6.486**	1.0		**0.495**	1.8	46	**0.056**	2.4	5	0.11	**3.977**	3.1	367	0.811	*98.7*	**121.7**	8.3	151.0			45.4	89–248
BM_5_a1	**2.582**	0.9		**0.225**	1.8	27	**0.040**	2.5	5	0.18	**3.118**	3.1	373	0.776	*81.9*	**105.5**	8.0					
BM_5_a2	**5.302**	0.9		**0.464**	1.8	32	**0.084**	2.4	6	0.18	**5.828**	3.1	396	0.826	*82.2*	**99.5**	6.3					
BM_5_a3	**2.335**	1.0		**0.217**	1.8	26	**0.047**	2.4	6	0.22	**2.986**	3.1	356	0.769	*76.3*	**99.3**	7.8					
BM_5_a4	**0.310**	1.4		**0.005**	11.6	1	**0.001**	224.6	0	0.17	**2.333**	3.1	453	0.756	*103.1*	**136.2**	15.0	**110.1**	**8.8**	**17.6**	16.0	
BM_11_a1	**2.094**	0.9		**0.147**	1.8	23	**0.020**	2.6	3	0.14	**2.295**	3.1	354	0.750	*101.2*	**135.0**	11.3					
BM_11_a2	**4.282**	0.9		**0.052**	2.1	9	**0.027**	2.5	5	0.52	**3.555**	3.1	603	0.760	*398.6*	**524.5**	42.4					
BM_11_a3	**2.746**	0.9		**0.033**	2.4	4	**0.006**	2.8	1	0.20	**5.578**	3.1	625	0.778	*281.0*	**361.2**	29.0	340.2			57.5	135–525

Measured He volumes, U, Th and Sm masses, and Ft-corrected He-ages in bold. Uncorrected He-ages in italics

Table 5 (U–Th)/He data from Dalhousie University (Canada)

Reduced (U–Th[Sm])/He data															Dispersion (1s/mean age) (%)	Range (given if dispersion > 20%)
Sample	Mineral	U (ppm)	Th (ppm)	^{147}Sm (ppm)	[U]e	Th/U	He (nmol/g)	Mass (µg)	Ft	ESR	Raw age, Ma	err., Ma	Corrected age			
													Age, Ma	1s, Ma		
BM 14	Apatite	14.9	14.5	66.7	18.6	0.97	3.3	8.08	0.78	70.60	31.90	0.17	40.9	1.23		
BM 14	Apatite	25.1	15.1	111.4	29.1	0.60	13.1	12.86	0.81	82.48	81.87	0.44	100.7	3.02		
BM 14	Apatite	25.8	24.2	139.0	32.0	0.94	5.6	4.83	0.74	58.35	31.65	0.18	42.9	1.29		
BM 14	Apatite	14.6	22.8	101.8	20.3	1.57	5.7	5.45	0.74	59.94	50.76	0.27	68.6	2.06		
BM 14	Apatite	24.1	18.1	111.7	28.9	0.75	11.6	7.56	0.77	65.79	72.71	0.41	94.8	2.84	40.3	41–101
BM 40	Apatite	60.2	35.8	458.9	70.7	0.60	30.6	5.02	0.73	55.50	77.89	0.47	106.8	3.20		
BM 40	Apatite	43.0	15.4	439.1	48.7	0.36	38.6	8.19	0.78	69.72	141.06	0.83	179.9	5.40		
BM 40	Apatite	25.9	30.2	324.7	34.5	1.17	10.1	4.22	0.72	55.26	52.52	0.30	72.7	2.18		
BM 40	Apatite	22.1	23.1	291.6	28.9	1.04	12.0	5.31	0.74	59.93	73.69	0.41	99.1	2.97		
BM 40	Apatite	26.9	17.1	329.5	32.4	0.64	11.1	7.15	0.76	63.16	61.24	0.36	80.6	2.42	39.5	73–180
BM 43	Apatite	15.3	35.2	310.7	25.0	2.30	5.7	3.38	0.69	50.26	40.21	0.23	58.2	1.74		
BM 43	Apatite	25.2	19.9	369.2	31.6	0.79	11.4	6.39	0.75	60.13	63.84	0.37	85.5	2.57		
BM 43	Apatite	23.7	15.7	333.4	28.9	0.66	10.3	8.78	0.79	72.25	63.26	0.35	80.3	2.41		
BM 43	Apatite	2.8	21.3	182.5	8.6	7.56	0.9	5.04	0.73	60.35	18.24	0.11	24.9	0.75		
BM 43	Apatite	5.6	34.4	273.6	14.9	6.15	2.9	3.27	0.70	52.16	33.15	0.20	47.7	1.43	41.7	25–86
BM 46	Apatite	18.1	40.0	363.3	29.1	2.21	7.8	7.92	0.77	69.63	47.50	0.23	61.6	1.85		
BM 46	Apatite	15.1	36.6	397.7	25.5	2.43	8.0	7.50	0.76	66.47	54.62	0.26	71.8	2.15		
BM 46	Apatite	18.0	56.3	475.8	33.3	3.12	29.6	4.71	0.72	56.84	154.10	0.77	213.4	6.40		
BM 46	Apatite	50.5	104.6	675.4	78.0	2.07	20.6	5.15	0.74	59.29	47.13	0.24	64.1	1.92		
BM 46	Apatite	16.0	54.2	400.4	30.5	3.39	10.8	3.61	0.69	51.42	62.06	0.33	89.3	2.68	64.3	62–213
BM 54	Apatite	6.4	14.1	684.2	13.0	2.21	7.4	8.72	0.77	70.75	89.45	0.45	115.4	3.46		
BM 54	Apatite	3.4	19.2	518.9	10.4	5.63	6.7	5.98	0.75	64.75	101.33	0.56	135.0	4.05		
BM 54	Apatite	4.1	22.4	409.6	11.3	5.48	3.6	4.74	0.72	57.01	52.18	0.30	72.5	2.17		
BM 54	Apatite	4.0	16.8	539.4	10.5	4.22	2.5	6.39	0.75	64.23	36.71	0.20	48.9	1.47		
BM 54	Apatite	2.5	14.8	409.8	7.9	5.95	1.6	7.45	0.76	68.48	30.94	0.17	40.5	1.22	50.1	41–135

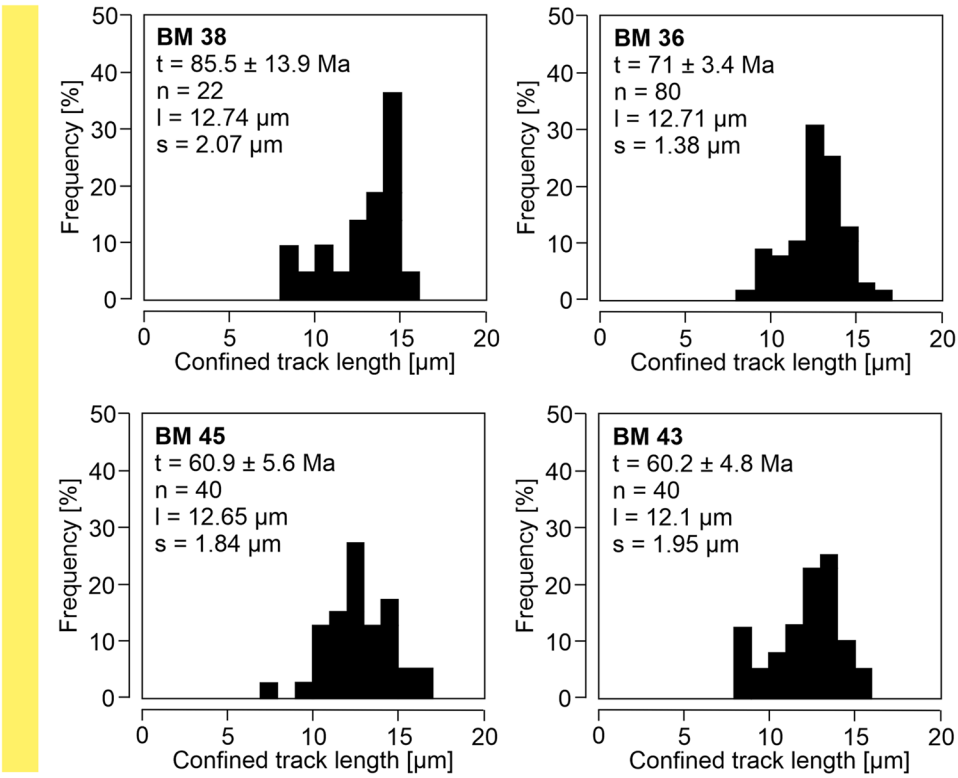

Fig. 7 Frequency distributions of confined spontaneous track lengths in apatite for samples with Late Cretaceous and Paleocene AFT ages. The yellow bar on the left side corresponds to the yellow color indicating the Early Cretaceous to Palaeocene age interval in Figs. 3 and 4

Quaternary gravel terraces of the Danube represent climatically and uplift controlled steps of fluvial incision.

The sedimentary record of preserved formations in the vicinity of the Bohemian Massif demonstrates that substantial reburial of the Variscan basement may have occurred during the Late Jurassic and/or Late Cretaceous. But the Early Cretaceous must have been a period of persistent regional erosion under a tropical climate. However, the total thicknesses of sedimentary overburden and precise delimitations of erosion and sedimentation areas are unknown. Thus, reconstructions of Mesozoic paleogeography yield only 'soft constraints' for thermochronological modeling. A rather 'strong constraint' is given for those samples, which were taken close to the base of the St. Marein-Freischling Formation (Oligocene). These rocks must have reached very shallow depth about 30 Ma ago, and significant reburial is excluded due to the formation's limited thickness.

Thermochronological modeling and general discussion

According to Gleadow et al. (1986b), mean confined track lengths around 12 and 13 µm and standard deviations between 1.2 and 2.0 µm are typical for undisturbed basement that underwent steady denudation.

Thus, our AFT ages, mean confined fission-track lengths (from 11.99 to 13.40 µm) and standard deviations (from 1.38 to 2.07 µm) do not contradict the assumption of slow steady cooling through the partial annealing zone (PAZ). However, the shape of some histograms is not negatively skewed, and some histograms are even bimodal (Figs. 5, 6, 7). Therefore, more complex cooling paths must be considered for some samples and age groups.

In a first interpretation step, we assume that the distinct frequency maximum of AFT ages between ca. 145 and 100 Ma represents cooling ages, i.e., that the samples underwent rather fast and continuous cooling through the whole AFT partial annealing zone between ca. 120 and 60 °C (cf. Wagner and Van den haute 1992). The AFT ages above 200 Ma probably represent post-Variscan cooling ages, while the AFT ages between 200 and 145 Ma may be mixed ages that are either the result of stepwise cooling or the result of moderate reheating between a late-Variscan and an Early Cretaceous cooling event. Such moderate reheating could have been caused by a Late Jurassic sedimentary reburial, as has been outlined in the previous chapter.

Figures 4 and 6 show that the confined track lengths of most samples of the age group between 145 and 100 Ma have rather high arithmetic means above 12.8 µm, while those of the other age groups (> 145 Ma and < 100 Ma) are mainly lower than 12.8 µm. This underlines the foregoing assumption that the frequency maximum of AFT ages between ca. 145 and 100 Ma coincides with a regional cooling event during the Early Cretaceous. Samples of the lowermost age

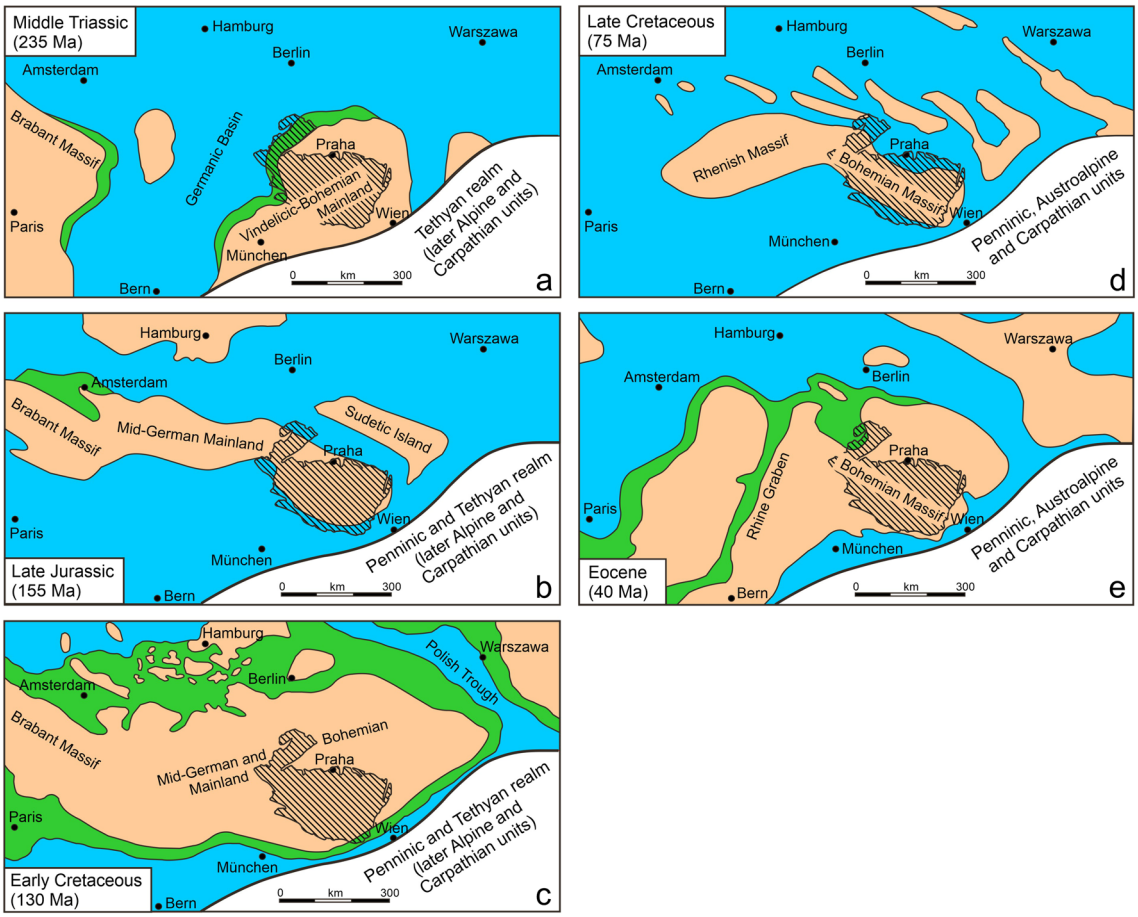

Fig. 8 Simplified palaeogeography of Middle Europe during the Middle Triassic (**a**), the Late Jurassic (**b**) the Early Cretaceous (**c**), the Late Cretaceous (**d**), and the Eocene (be), after Ziegler (1990), Faupl (1997) and Park (2014). The hatched area corresponds to the present-day outcropping basement shown in Fig. 1

group (< 100 Ma) have mean lengths of less than 12.75 µm and—except for sample BM 36—rather high standard deviations (> 1.8 µm). This indicates that the samples with ages of less than 100 Ma have not cooled continuously through the whole PAZ in Cenozoic times but did already reside at temperatures below 120 °C during the Middle and Late Cretaceous.

The outlined Mesozoic and Cenozoic palaeogeography helps to formulate rather 'strong' and 'weak' constraints for modeling of thermal histories. The fact that a thin cover of Oligocene freshwater sediments occurs along the Thaya and Kamp rivers on top of the Variscan basement yields a strong constraint for the potential cooling paths of adjacent basement rocks. The basement underneath or close to the St. Marein-Freischling formation (mainly between the towns of Gmünd and Horn) must have been close to the surface at about 30 Ma ago. On the other hand, the Mesozoic palaeogeography of already eroded formations on top of the Bohemian Massif is not well known. An Upper Jurassic and/or Middle Cretaceous to Campanian sedimentary cover may have buried marginal parts of the Bohemian Massif, but both sedimentary thicknesses and the position of ancient coastlines remain doubtful. Thus, potential reburial and reheating between ca. 100 to 80 Ma (Cenomanian to Campanian) may be considered as weak constraint. At least strong erosion of the hinterland is rather unlikely for the quoted time interval.

We used the program HeFTy (version 2.0.9, 2022 provided by Richard A. Ketcham) for inverse modeling of AFT data and AHe ages with dispersion below 20%. This program calculates the range of thermal histories (temperature versus time) that are potentially consistent with measured thermochronometric data (AFT age, frequency distribution of confined track lengths and AHe age) and with constraints that are imposed to the *t–T* path by use of independent geological evidence. Annealing kinetics of the AFT system rely on the investigations of Carlson et al. (1999), Donelick et al. (1999) and Ketcham et al. (1999), and on the improved model of Ketcham et al. (2007). Inverse modeling of AHe data uses the He diffusion kinetic model of Flowers et al. (2009). Random paths were generated by a Monte Carlo scheme

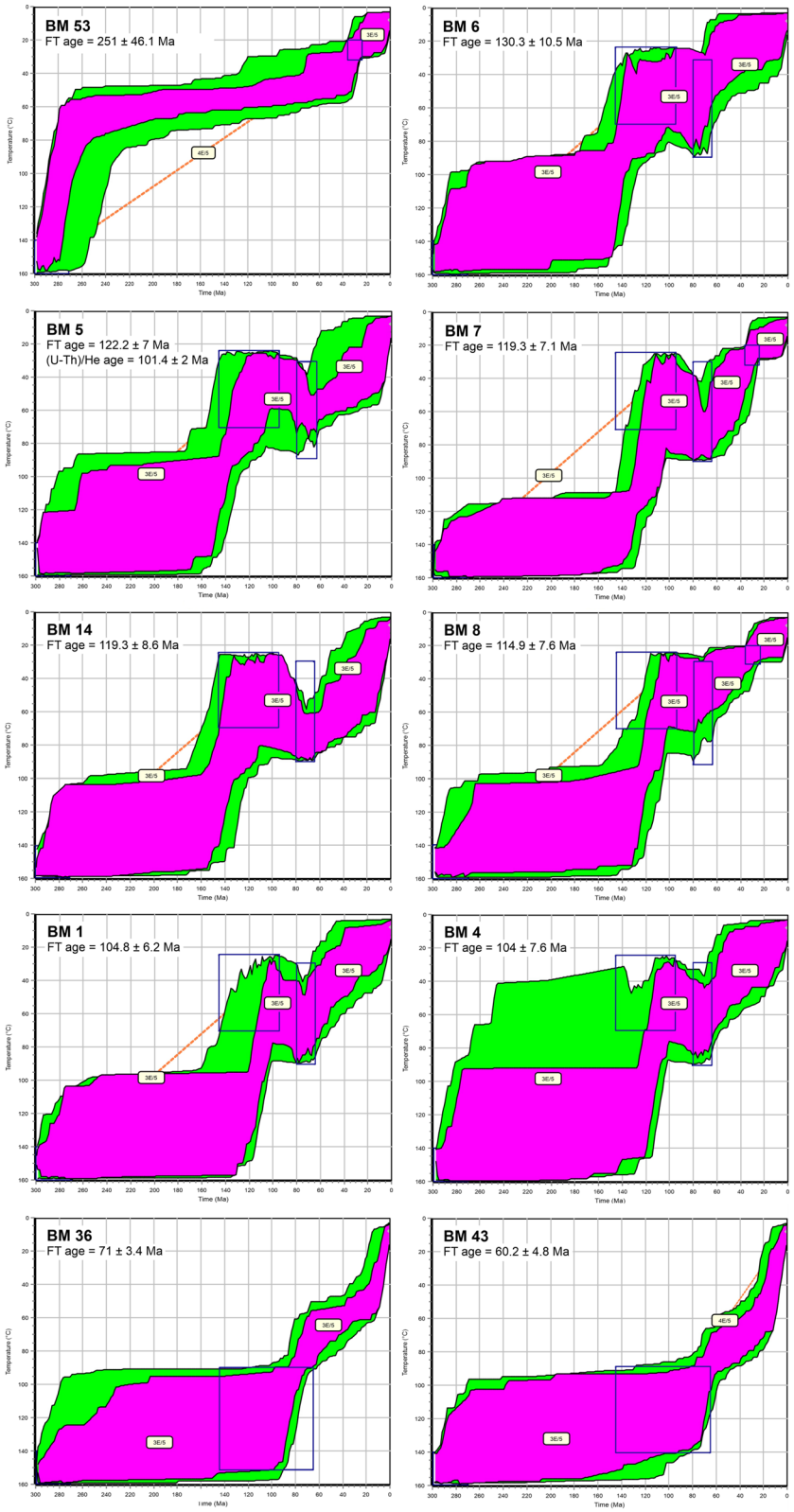

Fig. 9 Inversion models (temperature versus time) generated with HeFTy software (version 2.0.9, Richard A. Ketcham) for samples BM 53, 6, 5, 7, 14, 8, 1, 4, 36, and 43 (in descending order of AFT ages). Technical specifications: annealing model of Ketcham et al. (2007); goodness-of-fit (GOF) by Kolmogorov–Smirnov test; Monte Carlo method of search; random subsegment spacing between constraints; $|dT/dt| < 5$ °C/Ma for each subsegment; cf. text for geological constraints. The inverse model of BM 5 includes the concordant (U–Th)/He age as additional thermochronometer (calibration after Flowers et al. 2009)

with random spacing of sub-segments. We have imposed a maximum $|dT/dt|$ of 5 °C/Ma because exhumation and/or sedimentary burial rates of more than ca. 200 m/Ma are improbable for a non-orogenic setting. We have estimated the apatite's resistance to track annealing by including the diameters of etch pits parallel to the crystallographic c-axis (Dpar values in Table 2).

We have not measured the angle between confined tracks and the crystallographic c-axis because the apatite grains were embedded in epoxy in random orientation. A systematic assessment of such angles would have restricted the length measurements to those grains viewed perpendicular to the c-axis. In our case, most grains have a low length–width ratio. The right orientation is rare, and only few confined tracks would have been suitable for both length and angle measurement. Thus, we opted for a modeling procedure without taking angles into account. In this case, the HeFTy modeling routine is based on the assumption that confined tracks were chosen randomly for length measurement—regardless of track and grain orientation—and that no systematic bias has occurred.

For each path, the resulting AFT age and length distribution were calculated, and the goodness-of-fit (G.O.F.) between calculated and measured data was evaluated by a Kolmogorov–Smirnov test. In the case of sample BM 5, concordant AHe data have been included in the inverse model, i.e., in the estimation of G.O.F. values, but the other inverse models include AFT data only. The program HeFTy maps out time–temperature regions with "good" and "acceptable" fit, corresponding to G.O.F. values from 0.5 to 1 and from 0.05 to 0.5, respectively. Inverse modeling was terminated when at least 100 "good paths" had been found (inversion models of Fig. 9).

Depending on the geological setting of the sample, constraints were imposed on the modeled thermal histories. These constraints are based on geological observations, such as sedimentary horizons discordantly overlying basement rocks, thus proving subaerial unroofing previous to the time of deposition. They are defined by a series of boxes in the time–temperature graph. The starting and end point of each path segment must be located in these boxes. For all model runs, a present-day surface temperature of 8 ± 5 °C was imposed as constraint. This temperature is an estimation of the mean annual temperature during the last ca. 10 ka.

We imposed 20–30 °C at 35–25 Ma for samples from locations close to discordant contact with the St. Mareien-Freischling Formation (BM 53, 7 and 8). Thermal histories of samples of the AFT age group between 145 and 100 Ma (BM 1, 4, 5, 6, 7, 8 and 14) were allowed to reach low temperatures in the Early to Middle Cretaceous (between 145 and 95 Ma) and to be moderately reheated in the Late Cretaceous with a temperature climax between 80 and 65 Ma. These constraints were rather soft because of a broad temperature spread and a large time interval of the boxes (25–70 °C between 145 and 95 Ma; 30–90 °C). In other words, Late Cretaceous reheating was enabled but not enforced. Stepwise cooling or even continuous cooling would have been compatible with these weak constraints. Two samples of the AFT age group with the lowest ages (BM 36 and 46) were modeled without the option of cooling to less than 60 °C in Cretaceous times. Inverse modeling with a constraining box of 90–150 °C from 145 to 65 Ma produced a much higher percentage of cooling histories with "good" fit than unconstrained modeling from 300 Ma to the present.

Inverse modeling of sample BM 53 (Fig. 9) indicates fast post-Variscan cooling during the Late Carboniferous and the Early Permian. The sample resided at ca. 60 °C from 250 to 70 Ma, before cooling became faster again. Good fit was obtained without Late Cretaceous reburial, but the inverse model is compatible with stepwise cooling after ca. 70 Ma.

Inverse modeling of samples with Early Cretaceous AFT ages (BM 6, 5, 7, 14, 8, 1 and 4, in descending order of the AFT ages) was performed with the weak constraints mentioned above that allow Early Cretaceous surface approach and subsequent reheating during the Late Cretaceous (Fig. 9). These models indicate that most samples did not cool to less than 100 °C before ca. 145 Ma ago. Fast cooling occurred during the Early Cretaceous. Afterward, the samples were either moderately reheated or resided at a fairly constant temperature until ca. 65 Ma ago. The inverse model of BM 5 with included AHe data most narrowly confines good fit and depicts distinct Late Cretaceous reheating. Cenozoic cooling was again faster. Some samples (BM 5, 7, 14 and 8) show a last step of accelerated cooling after ca. 30 Ma ago.

Inverse modeling of samples with Paleogene AFT ages (BM 36 and 46) was performed without Cenozoic time–temperature constraints, but cooling to less than 90 °C was prevented for the whole Cretaceous (Fig. 9) because test runs without this constraint produced a lesser percentage of "good" fit. This supports the assumption that the samples resided in the PAZ until the end of the Cretaceous. The resulting models indicate stepwise cooling after ca. 80 Ma. Fast cooling from 80 to 60 Ma is followed by a period of moderate cooling from 60 to 20 Ma, and a second period of fast cooling after 20 Ma. The area of good fit would allow for a moderate reheating between 100 and 80 Ma but does not imply it.

Accelerated basement exhumation in latest Cretaceous or earliest Paleogene times is also indicated by independent geological evidence: Heavy mineral spectra in Late Cretaceous and Paleogene sediments of the Rhenodanubian flysch exhibit a distinct compositional change at the Cretaceous/Paleogene boundary. Associations rich in garnet dominate in Campanian and Maastrichtian flysch sandstones (Woletz 1963). The source rocks of these garnets can be found in the metamorphosed units of the Austroalpine hinterland. This supply of garnet-rich detritus terminated at the end of the Cretaceous and was replaced by sandy material rich in zircon, typical for Paleogene sandstones of the Flysch zone and the Helveticum (Woletz 1963). This sudden change in detritus supply is best explained by the progressive closure

of the North Penninic Ocean and the increasing terrigeneous input from its northern margin, i.e., from the European shelf and the adjacent crystalline—mainly granitic—basement of the Bohemian Massif. This scenario is compatible with the development of a continental escarpment along the NW–SE trending Weinsberg ridge. The southern margin of the Bohemian Massif was buried under a thick cover of marine and coastal sediments during the Late Cretaceous. The transgression culminated in the Campanian. Afterward, the sea level dropped, and the sedimentary overburden on the southern Bohemian Massif was removed by erosion. In large areas, Weinsberg and other Variscan granites were exposed during the Paleogene and delivered zircon-bearing sand to the European shelf, the Helveticum and turbiditic fans of the North Penninic Ocean. The continental escarpment on the northern (passive) margin of the Flysch Ocean developed from about 60 to 35 Ma ago, i.e., during a time span of ca. 35 Ma. This situation ended in the Late Eocene, when the Austroalpine nappe pile collided with the European shelf.

A last phase of accelerated cooling at ca. 20 Ma is implied by thermal simulations of samples 5, 36 and 43. Interestingly, the sedimentary archive of the eastern part of the Molasse basin records a change in the sedimentation pattern and onset of rapid basin infill at ca. 19 Ma (Kuhlemann 2007; Hülscher et al. 2019). Concurrent exhumation of the nearby Alpine source area is indicated by fully reset AFT ages ranging from ca. 18 to 25 Ma from the easternmost flysch zone W of Vienna (Trautwein et al. 2001). New AHe data from clastic formations of the nappe pile of the Northern Calcareous Alps in the easternmost Eastern Alps confirm such a young cooling pulse (Heberer et al. 2022). It may be correlated with thrust activity of the advancing nappe stack (e.g., Beidinger and Decker 2014), but it may also, at least partly, be the surficial expression of more deep-seated processes. Based on the AlpArray seismological campaign, Handy et al. (2021) proposed a new model of slab configuration beneath the Alps, including a completely detached slab beneath the Eastern Alps.

With regard to domal uplift on a lithospheric scale, as it has been proposed by von Eynatten et al. (2021) for major areas of central Europe, we have to consider the regional size and amplitude of the exhumed areas. The NW–SE trending ridge of the Weinsberg Forest has a length of about 80 km, and its width in NE–SW direction is even smaller (Fig. 2b). Thus, the horizontal size of this topographic feature is only twice as much as the crustal thickness. It is rather unlikely that exhumation produced by lithospheric folding (Cloetingh and Burov 2011; Cloetingh et al. 1999) or dynamic topography caused by mantle upwelling (Braun et al. 2013) may generate a distinct differential exhumation on such a small scale. The observed asymmetry of measured AFT ages on both sides of the Weinsberg Forest is better explained by the development of an ancient escarpment from the latest Cretaceous (Maastrichtian) to the Eocene. During this time span of ca. 35 Ma, the southern Bohemian Massif and the adjacent shelf area formed a passive continental margin at the northeastern side of the North Penninic Ocean.

Prominent examples of escarpments on passive continental margins are those of the Drakensberg in South Africa (cf. Brown et al. 2002), the Transantarctic Mountains (cf. Fitzgerald and Gleadow 1990) and the Snowy Mountains in New South Wales (Australia; cf. Kohn et al. 1999). Their surface uplift, denudation rates, drainage evolution and erosional retreat are produced by fluvial incisions from the coast backward and by progressive isostatic rebound of the crust underneath the eroded coastal slopes. This process creates an asymmetric exhumation pattern at both sides of the crest. By means of backstacking AFT topography, Brown et al. (2002) have estimated 4.5 km of denudation for the coastal zone adjacent to the Drakensberg Escarpment in South Africa, which rises up to a present-day altitude of 3482 m. Maximum altitudes of the Weinsberg Forest are much smaller (up to 1053 m). But a cumulative exhumation of about 2000 m (including basement erosion and removal of a putative overburden of Upper Cretaceous sediments) since the latest Cretaceous would have been sufficient to bring rocks from a Late Cretaceous PAZ to the surface. With an assumed geothermal gradient of 30 °C/km, latest Cretaceous and Cenozoic erosion could have produced a regional cooling in the order of 60 °C on the sloping area to the SW of the crest. In addition to a Neogene surface temperature of ca. 15 °C, this cooling would correspond to initial rock temperatures of ca. 75 °C previous to latest Cretaceous and Cenozoic exhumation.

We propose the name of 'Weinsberg escarpment' for the Paleogene geomorphic situation on the southwestern slopes of the Weinsberg Forest. The term 'Danube escarpment' would be misleading, because the river Danube did not yet exist in the Paleogene and the original escarpment was not shaped by the present-day fluvial catchment.

After the closure of the North Penninic Ocean, during the Late Eocene, either collisional coupling of the advancing Alpine-Carpathian nappe stack with its northern foreland (Ziegler and Dèzes 2007) or—more likely—East-Alpine slab detachment (Handy et al. 2021) may have caused accelerated uplift, exhumation and cooling during the latest 20 Ma.

Conclusions

The regional distribution of AFT ages, the synopsis of already known paleogeographical reconstructions, as well as inverse modeling of both AFT and concordant AHe data lead to the following conclusions:

1. The area from the top of the Weinsberg Forest down to the Kamp valley to the E of Zwettl has experienced strong and uniform erosion during the Early Cretaceous. This event gave rise to quite homogeneous AFT ages between ca. 145 and 100 Ma.
2. No AFT age breaks occur at the late Variscan Diendorf and Vitis faults. Important vertical offset along these faults during the Cretaceous and Cenozoic is thus precluded.
3. Shallow-marine and terrestrial sediments have reburied large areas of the southern Bohemian Massif during the Late Cretaceous, until the Campanian. This cover protected a former weathering basal relief from later erosion. Morphological remnants of this Mesozoic weathering basal relief are preserved as 'sealed relief' until present. The Late Cretaceous reburial and reheating caused broad and even bimodal frequency distributions of confined track lengths in apatite, but did not produce a full reset of the AFT and AHe systems.
4. The regional asymmetry of measured AFT ages relative to the NW–SE trending ridge of the Weinsberg Forest is not compatible with the geomorphological model of a piedmont staircase, which would require uplift en bloc, similar exhumation rates on both sides of the ridge, and similar cooling ages at similar altitude on both sides of the ridge.
5. Large-scale domal uplift of the Variscan basement may have produced Early Cretaceous exhumation but is ruled out for Cenozoic time because of the quoted regional asymmetry around the highest summits of the Weinsberg Forest.
6. The sloping area between the Weinsberg Forest and the Danube started to develop as an escarpment on a passive continental margin adjacent to the North Penninic Ocean. In latest Cretaceous (Maastrichtian) and Paleogene times, this 'Weinsberg escarpment' formed the transition between the shelf area and the elevated peneplain on top of the Weinsberg Forest. Present-day surface rocks of this sloping area did already reside in the apatite PAZ before their final Cenozoic exhumation.
7. Either collisional coupling of the East-Alpine and Carpathian orogens with their northern foreland or slab detachment underneath the Eastern Alps caused a final accelerated exhumation that started ca. 20 Ma ago—especially in the sloping area to the NE of the Danube.

Supplementary Information The online version contains supplementary material available at https://doi.org/10.1007/s00531-023-02294-6.

Acknowledgements We appreciate scientific suggestions and critical remarks of Friedrich Finger and an anonymous reviewer. Both reviews were valuable for the improvement of the manuscript.

Author contributions All authors contributed to the study conception and design. Sampling, data collection and analysis were performed by Ewald Hejl, Bianca Heberer and Gert Sekyra. The first draft of the manuscript was written by Ewald Hejl and Bianca Heberer, and was approved by all authors.

Funding Open access funding provided by Paris Lodron University of Salzburg. This research was supported by OP RDE [grant number CZ. 02.1.01/0.0/0.0/16_026/0008459 (Geobarr) from the ERDF].

Data availability The authors confirm that the data supporting the findings of this study are available within the article and its supplementary materials.

Declarations

Conflict of interest The authors declare no conflict of interest. The funders had no role in the design of the study; in collection, analyses, or interpretation of data; in writing of the manuscript, or in the decision to publish the results.

References

Aramowicz A, Anczkiewicz AA, Mazur S (2006) Fission track dating of apatites from the Góry Sowie Massif, Polish Sudetes, NE Bohemian Massif: implications of post-Variscan denudation and uplift. N Jb Miner Abh 182(3):221–229

Beidinger A, Decker K (2014) Quantifying Early Miocene in-sequence and out-of-sequence thrusting at the Alpine-Carpathian junction. Tectonics 33(2):222–252

Borger H (1992) Paleotropical weathering on different rocks in Southern Germany. Zeitschr Geomorph N F Suppl 91:95–108

Botor D (2014) Timing of coalification of the Upper Carboniferous sediments in bm,, the Upper Silesia Coal Basin (SW Poland) on the basis of apatite fission-track and helium dating. Gospod Surow Mineralnymi (Miner Resour Manag.) 30/1:85–104

Botor D, Dunkl I, Anczkiewicz A, St M (2017) Post-Variscan thermal history of the Moravo-Silesian lower Carboniferous (NE Czech Republic–SW Poland). Tectonophysics 712–713:643–662. https://doi.org/10.1016/j.tecto.2017.06.035

Brandmayr M, Dallmeyer RD, Handler R, Wallbrecher E (1995) Conjugate shear zones in the Southern Bohemian Massif (Austria)—implications for Variscan and Alpine tectonothermal activity. Tectonophysics 248:97–116

Braun J, Robert X, Simon-Labric T (2013) Eroding dynamic topography. Geophys Res Lett 40:1494–1499

Brodie J, White N (1994) Sedimentary basin inversion caused by igneous underplating: Northwest European continental shelf. Geology 22:147–150

Brown RW, Summerfield MA, Gleadow AJW (2002) Denudational history along a transect across the Drakensberg Escarpment of southern Africa derived from apatite fission track thermochronology. J Geophys Res Solid Earth 107(B12):2350. https://doi.org/10.1029/2001JB000745

Büdel J (1957) Die „doppelten Einebnungsflächen" in den feuchten Tropen. Zeitschr Geomorph N F 1:201–208

Carlson WD, Donelick RA, Ketcham RA (1999) Variability of fission-track annealing kinetics I: experimental results. Am Mineral 84:1213–1223

Cloetingh S, Burov E (2011) Lithospheric folding and sedimentary basin evolution: a review and analysis of formation mechnaisms. Basin Res 23:257–290

Cloetingh S, Burov E, Poliakov A (1999) Lithosphere folding: Primary response to compression? (from central Asia to Paris basin). Tectonics 18:1064–1083

Cloos H (1925) Einführung in die tektonische Behandlung magmatischer Erscheinungen. 1. Spezieller Teil. Das Riesengebirge in Schlesien. Borntraeger, Berlin, XI + 194 p

Danišik M, Štěpančiková P, Evans NJ (2012) Constraining long-term denudation and faulting history in intraplate regions by multi-system thermochronology—an example of the Sudetic Marginal Fault (Bohemian Massif, Central Europe). Tectonics 31:1–19. https://doi.org/10.1029/2011TC003012

Donelick RA, Ketcham RA, Carlson WD (1999) Variability of fission-track annealing kinetics II: crystallographic orientation effects. Am Miner 84:1224–1234

Eberts A, Fazlikhani H, Bauer W, Stollhofen H, de Wall H, Gabriel G (2021) Late to post-Varican differential uplift and basement segmentation along the SW Bohemian Massif. Central Europe Solid Earth 12(10):2277–2301

Farley KA (2000) Helium diffusion from apatite: general behavior as illustrated by Durango fluorapatite. J Geophys Res Solid Earth 105(B2):2903–2914

Farley KA, Wolf RA, Silver LT (1996) The effects of long alpha-stopping distances on (U–Th)/He ages. Geochim Cosmochim Acta 60(21):4223–4229

Faupl P (1997) Historische geologie. WUW Universitätsverlag, Wien, p 270

Fazlikhani H, Bauer W, Stollhofen H (2022) Variscan structures and their control on latest to post-Variscan basin architecture: insights from the westernmost Bohemian Massif and southeastern Germany. Solid Earth 13:393–416. https://doi.org/10.5194/se-13-393-2022

Finger F, Riegler G (1999) Der Thayabatholith und der kristalline Untergrund des Weinviertels. Arbeitstagung der Geol. B.-A. Retz-Hollabrunn, Wien, pp 23–30

Finger F, Gerdes A, Janoušek V, René M, Riegler G (2007) Resolving the Variscan evolution of the Moldanubian sector of the Bohemian Massif: the significance of the Bavarian and the Moravo-Moldanubian tectonometamorphic phases. J Geosci 52:9–28. https://doi.org/10.3190/jgeosci.005

Finger F, Schiller D, Lindner M, Hauzenberger Ch, Verner K, Žák J (2022) Ultrahigh-temperature granites and a curious thermal eye in the post-collisional South Bohemian batholith of the Variscan orogenic belt (Europe). Geology 50(5):542–546

Fischer H (1979) Reliefgenerationen im Kristallinmassiv, Donauraum, Alpenvorland und Alpenrand im westlichen Niederösterreich. Forsch Dt Landesk 213:1–232

Fitzgerald PG, Gleadow AJW (1990) New approaches in fission track geochronology as a tectonic tool: examples from the Transantarctic Mountains. Nucl Tracks Rad Meas 17:351–357. https://doi.org/10.1016/1359-0189(90)90057-5

Flowers RM, Ketcham RA, Shuster DL, Farley KA (2009) Apatite (U–Th)/He thermochrono-metry using a radiation damage accumulation and annealing model. Geochim Cosmochim Acta 73(8):2347–2365

Flowers RM, Ketcham RA, Enkelmann E, Gautheron C, Reiners PW, Metcalf JR, Danišik M, Stockli DF, Brown RW (2022a) (U–Th)/He chronology: Part 2. Considerations for evaluating, integrating, and interpreting conventional individual aliquot data. GSA Bull. https://doi.org/10.1130/B36268.1

Flowers RM, Zeitler PK, Danišik M, Reiners PW, Gautheron C, Ketcham RA, Metcalf JR, Stockli DF, Enkelmann E, Brown RW (2022b) (U–Th)/He chronology: Part 1. Data, uncertainty, and reporting. GSA Bull Spec Vol Rep Interpr Geochronol Data. https://doi.org/10.1130/B36266.1

Frasl G, Finger F (1991) Geologisch-petrographische Exkursion in den österreichischen Teil des Südböhmischen Batholiths. Eur J Mineral 3(Suppl. 2):23–40

Friedl G (1997) U/Pb-Datierungen an Zirkonen und Monaziten aus Gesteinen vom österreichischen Anteil der Böhmischen Masse. Dissertation Naturwiss. Fak. Univ. Salzburg, p 242

Friedl G, von Quadt A, Finger F (1994) 340 Ma U/Pb-Monazitalter aus dem niederösterreichischen Moldanubikum und ihre geologische Bedeutung. Terra Nostra 3(94):43–46

Friedl G, Finger F, McNaughton NJ, Fletcher IR (2000) Deducing the ancestry of terranes: SHRIMP evidence for South America-derived Gondwana fragments in Central Europe. Geology 28:1035–1038

Friedl G, Finger F, Paquette J-L, von Quadt A, McNaughton NJ, Fletcher IR (2004) Pre-Variscan geological events in the Austrian part of the Bohemian Massif deduced from U-Pb zircon ages. Int J Earth Sci (geol Rundsch) 93:802–823

Friedl G, Cooke RA, Finger F, McNaughton NJ, Fletcher IR (2011) Timing of Variscan HP-HT metamorphism in the Moldanubian Zone of the Bohemian Massif: U-Pb SHRIMP dating on multiply zoned zircons from a granulite from the Dunkelsteiner Wald Massif, Lower Austria. Miner Petrol 102:63–75

Galliker D, Hugentobler E, Hahn B (1970) Spontane Kernspaltung von ^{238}U und ^{241}Am. Helv Phys Acta 43:593–606

Gautheron C, Tassan-Got L, Barbarand J, Pagel M (2009) Effect of alpha-damage annealing on apatite (U–Th)/He thermochronology. Chem Geol 266(3–4):157–170

Gebauer D, Friedl G (1993) A 1.38 Ga protolith age for the Dobra orthogneiss (Moldanubian zone of the southern Bohemian massif, NE Austria): evidence ion-microprobe (SHRIMP)-dating of zircon. Eur J Miner 5:115

Gilbert GK (1904) Domes and dome structure of the high sierra. Bull Geol Soc Am 15:29–36

Glasmacher AU, Mann U, Wagner GA (2002) Thermotectonic evolution of the Barrandian, Czech Republic, as revealed by apatite fission-track analysis. Tectonophysics 359:381–402

Gleadow AJW (1981) Fission-track dating methods: what are the real alternatives? Nucl Tracks Rad Meas 5:3–14

Gleadow AJW, Duddy IR, Green PF, Hegarty KA (1986a) Fission-track lengths in apatite annealing zone and the interpretation of mixed ages. Earth Planet Sci Lett 78:245–254

Gleadow AJW, Duddy IR, Green PF, Lovering JF (1986b) Confined fission track lengths in apatite: a diagnostic tool for thermal history analysis. Contrib Miner Petrol 94(4):405–415

Green PF (1985) Comparison of zeta base lines for fission track dating of apatite, zircon and sphene. Chem Geol (isotope Geosci Sect) 58:1–22

Gyurits K, Kurzweil H (1976) Grobkornsedimentation der pannonen Donau in Österreich am Beispiel der Mistelbacher Schotter. Tschermaks Miner Petrogr Mitt 23:233–249

Handy MR, Schmid SM, Paffrath M, Friederich W, AlpArray Working Group (2021) Orogenic lithosphere and slabs in the greater Alpine area—interpretations based on teleseismic P-wave tomography. Solid Earth 12(11):2633–2669

Heberer B, Salcher B, Dunkl I, Sachsenhofer R, Wagreich M, Wessely G (2022) An Oligocene to Miocene cooling pulse in the easternmost Alps detected by thermochronology—a result of thrust tectonics and/or deep mantle processes? In: Rantitsch G, Raith JG (eds) PANGEO Austria 2022—abstracts, 10–14 September 2022, Leoben. Berichte Geol Bundesanstalt, vol 143, p 10

Hejl E, Ney P (1994) Flotationsverfahren zur Abtrennung von Apatit und Zirkon aus silikatischen Paragenesen. Mitt Österr Miner Ges 139:129–133

Hejl E, Coyle D, Lal N, van den haute P, Wagner G (1997) Fission-track dating of the western border of the Bohemian massif: thermochronology and tectonic implications. Int J Earth Sci (geol Rundsch) 86:210–219. https://doi.org/10.1007/s005310050133

Hejl E, Sekyra G, Friedl G (2003) Fission-track dating of the southeastern Bohemian massif (Waldviertel, Austria): thermochronology and long-term erosion. Int J Earth Sci (geol Rundsch) 92:677–690

Höck V (1975) Mineralzonen in Metapeliten und Metapsammiten der Moravischen Zone in Niederösterreich. Mitt Geol Ges 66(67):49–60

Höck V (1994) Moravian zone: metamorphic evolution. In: Dallmeyer RD, Franke W, Weber K (eds) Prepermian geology of Central and Eastern Europe. Springer, Berlin, pp 541–553

Huber KH (1996) Zum Formenschatz der Granitverwitterung und—abtragung im nordwestlichen Waldviertel. Das Waldviertel 45(1):111–130

Hülscher J, Fischer G, Grunert P, Auer G, Bernhardt A (2019) Selective recording of tectonic forcings in an oligocene/miocene submarine channel system: insights from new age constraints and sediment volumes from the austrian northern alpine foreland basin. Front Earth Sci 7:302. https://doi.org/10.3389/feart.201900302

Jonckheere R, Mars M, Van den haute P, Rebetetz M, Chambaudet A (1993) L'Apatite de Durango (Mexique): analyse d'un minéral standard pour la datation par traces de fission. Chem Geol 103:141–154

Jonckheere R, Van den haute P, Ratschbacher L (2015) Standardless fission-track dating of the Durango apatite age standard. Chem Geol 417:44–57

Ketcham RA, Donelick RA, Carlson WD (1999) Variability of apatite fission-track annealing kinetics III: Extrapolation to geological time scales. Am Miner 84:1235–1255

Ketcham RA, Carter AC, Donelick RA, Barbarand J, Hurford AJ (2007) Improved modelling of fission-track annealing in apatite. Am Miner 92:799–810

Kieslinger A (1964) Die Granitblöcke des Waldviertels. In: Machura L (ed) Die Blockheide Eibenstein bei Gmünd. Ein Naturpark im Waldviertel. Wien (NÖ Landesregierung), pp 4–8

Köhler W (1976) "Granitrestlinge" im Naturpark Blockheide-Eibenstein im niederösterreichischen Waldviertel. Aufschluß 27:319–320

Kohn BP, Gleadow AJW, Cox SJD (1999) Denudation history of the Snowy Mountains: constraints from apatite fission track thermochronology. Aust J Earth Sci 46:181–198

Kröner A, Wendt IJ, Liew TC, Compston W, Todt W, Fiala J, Vankova V, Vanek J (1988) U-Pb zircon and Sm-Nd model ages of high-grade Moldanubian sediments, Bohemian massif, Czechoslovakia. Contrib Mineral Petrol 99:257–266

Kuhlemann J (2007) Paleogeographic and paleotopographic evolution of the Swiss and Eastern Alps since the Oligocene. Glob Planet Change 58:224–236

Kuhlemann J, Kempf O (2002) Post-Eocene evolution of the North Alpine Foreland Basin and its response to Alpine tectonics. Sediment Geol 152:45–78

Leichmann J, Hejl E (1996) Quaternary tectonics at the eastern border of the Bohemian Massif: new outcrop evidence. Geol Mag 133:103–105

Lindner M, Dörr W, Reither D, Finger F (2020) The Dobra Gneiss and the Drosendorf Unit in the southeastern Bohemian Massif, Austria: West-Amazonian crust in the heart of Europe. Geol Soc Lond Spec Publ 503(1):SP503-2019-232

Malzer O, Rögl F, Seifert P, Wagner L, Wessely G, Brix F (1993) Die Molassezone und deren Untergrund. In: Brix F, Schultz O (eds) Erdöl und Erdgas in Österreich. Naturhistorisches Museum, Wien, pp 281–358

Meier T, Soomro RA, Viereck L, Lebedev S, Behrmann JH, Weidle C, Cristiano L, Hanemann R (2016) Mesozoic and Cenozoic evolution of Central European lithosphere. Tectonophysics 692:58–73

Niebuhr B, Pürner T, Wilmsen M (2009) Lithostratigraphie der außeralpinen Kreide Bayerns. Schriftenr Dt Ges Geowiss 65:7–58

Nielsen SB, Thomsen E, Hansen DL, Clausen OR (2005) Plate-wide stress relaxation explains European Palaeocene basin inversions. Nature 435:195–198

Ollier CD (1988) Deep Weathering, groundwater and climate. Geogr Ann Ser A 70(4):285–290

Park G (2014) The making of Europe. A geological history. Dunedin Academic Press, Edinburgh-London, p XII + 164

Pötzsch CG (1803) Bemerkungen und Beobachtungen über das Vorkommen des Granits in geschichteten Lagen und Bänken. Waltherische Hofbuchhandlung, Dresden, p XXXII + 554

Riedl H (2004) New contributions to the geomorphology of the Aegean archipelago in particular consideration of dating peneplains and pediments and their palaeoclimatic conditions. Ann Géol Pays Helléniq 1e Sér 40(A):11–49

Riedl H (2007) Zur Entwicklung der Piedmonttreppentheorie und ihrer Erkenntnisobjekte. Mitt Österr Geogr Ges 149:55–80

Roetzel R, Steininger FF (1996) Älteres Tertiär. Das Waldviertel 45(1):75–78

Schermann O (1966) Über Horizontalverschiebungen am Ostrand der Böhmischen Masse. Mitt Ges Geol Bergbaustud 16:89–103

Schnabel W, Krenmayr H-G, Mandl GW, Nowotny A, Roetzel R, Scharbert S (2002) Geologische Karte von Niederösterreich 1: 200.000. Legende und kurze Erläuterung. Geologische Bundesanstalt, Wien, p 47

Schröder B, Ahrendt H, Wemmer K (1997) Postvariscan sedimentation along the western margin of Bohemian Massif. Int J Earth Sci (geol Rundsch) 86:178–184

Shuster DL, Flowers RM, Farley KA (2006) The influence of natural radiation damage on helium diffusion kinetics in apatite. Earth Planet Sci Lett 249:148–161

Siebel W, Hann HP, Danišik M, Shang CK, Berthold C, Rohrmüller J, Wemmer K, Evans NJ (2009) Age constraints on faulting and fault reactivation: a multi-chronological approach. Int J Earth Sci (geol Rundsch) 99:1187–1197. https://doi.org/10.1007/s00531-009-0474-9

Sobczyk A, Sobel ER, Georgieva V (2020) Meso-Cenozoic cooling and exhumation history of the Orlica-Snieznik Dome (Sudetes, NE Bohemian Massif, Central Europe): Insights from apatite fission-track thermochronometry. Terra Nova 32:122–133. https://doi.org/10.1111/ter.12449

Spreitzer H (1951) Die piedmonttreppen in der regionalen geomorphologie. Erdkunde Arch Wiss Geogr 5:294–305

Steininger FF, Roetzel R (1996) Jüngeres Tertiär. Das Waldviertel 45(1):79–86

Suk M et al. (1984) Geological history of the territory of the Czech Socialist Republic. Praha Geological Survey, Praha, p 396

Thomson SM, Zeh A (2000) Fission-track thermochronology of the Ruhla crystalline complex: new constraints on the post-Variscan thermal evolution of the NW Saxo-Bohemian massif. Tectonophysics 324:17–35

Tollmann A (1985) Geologie von Österreich. Band II. Außerzentralalpiner Anteil. Deuticke, Wien, p XVI + 711

Trautwein B, Dunkl I, Frisch W (2001) Accretionary history of the Rhenodanubian flysch zone in the Eastern Alps—evidence from apatite fission-track geochronology. Int J Earth Sci (geol Rundsch) 90(3):703–713

Ulčný D (2001) Depositional systems and sequence stratigraphy of coarsegrained deltas in a shallow-marine, strike-slip setting: the Bohemian Cretaceous Basin, Czech Republic. Sedimentology 48:599–628

Ulčný D, Špičáková L, Grygar R, Svobodá M, Čech S, Laurin J (2009) Palaeodrainage systems at the basal unconformity of the Bohemian Cretaceous Basin: roles of inherited fault systems and basement lithology during the onset of basin filling. Bull Geosci 84(4):577–610

Unger HJ (1989) Die Lithozonen der Oberen Süßwassermolasse Südostbayerns und ihre vermutlichen zeitlichen Äquivalente gegen Westen und Osten. Geol Bavaric 94:195–237

Vamvaka A, Siebel W, Chen F, Rohrmüller J (2014) Apatite fission-track dating and low-temperature history of the Bavarian Forest (southern Bohemian Massif). Int J Earth Sci (geol Rundsch) 103:103–119. https://doi.org/10.1007/s00531-013-0945-x

Van den haute P, Jonckheere R, De Corte F (1988) Thermal neutron fluence determination for fission-track dating with metal activation monitors: a re-investigation. Chem Geol (isotope Geosci Sect) 73:233–244

Vasicek W (1991) Das Jungpaläozoikum von Zöbing. Exkursionen im Jungpaläozoikum und Mesozoikum Österreichs. Österr Paläont Ges, Wien, pp 1–21

Ventura B, Lisker F (2003) Long-term landscape evolution of the northeastern margin of the Bohemian Massif: apatite fission-track data from the Erzgebirge (Germany). Int J Earth Sci (geol Rundsch) 92:691–700

Ventura B, Lisker F, Kopp J (2009) Thermal and denudation history of the Lusatian Block (NE Bohemian Massif, Germany) as indicated by apatite fission-track data. In: Lisker F, Ventura B, Glasmacher UA (eds) Thermochronological methods: from palaeotemperature constraints to landscape evolution models, vol 324. Geol Soc London Spec Publ, London, pp 181–192

Vercoutere C (1994) The thermotectonic history of the Brabant massif (Belgium) and the Naab basement (Germany): an apatite fission-track analysis. PhD Thesis, Univ. Gent, Belgium

von Eynatten H, Kley J, Dunkl I, Hoffmann V-E, Simon A (2021) Late Cretaceous to Paleogene exhumation in central Europe—localized inversion vs. large-scale domal uplift. Solid Earth 12:935–958. https://doi.org/10.5194/se-12-9352021

Wagner G A, van den haute P (1992) Fission-track dating. Enke, Stuttgart, p XIV + 285

Wagner GA, Hejl E, van den haute P (1994) The KTB fission-track project: methodical aspects and geological implications. Radiat Meas 23:95–101

Wilhelmy H (1981) Klimamorphologie der Massengesteine. Wiesbaden, p 245

Woletz G (1963) Charakteristische Abfolgen der Schwermineralgehalte in Kreide- und Alttertiär-Schichten der nördlichen Ostalpen. Jb Geol B-A 106:89–119

Ziegler P (1990) Geological Atlas of Western and Central Europe. Shell Int. Petroleum Maatschappij B.V., Den Haag, p 239

Ziegler PA, Dèzes P (2007) Cenozoic uplift of Variscan Massifs in the Alpine foreland: timing and controlling mechanisms. Glob Planet Change 58:237–269